

Supplementary Material: Global Depths for Irregularly Observed Multivariate Functional Data

Zhuo Qu¹, Wenlin Dai² and Marc G. Genton¹

November 30, 2022

This supplementary material provides the results of Models 1-4 in the Simulation Studies and the proofs of theorems. In Section 1, we first present one simulation of all the above models with contamination but no sparseness. Next, we demonstrate the robustness of depths from extracting the median and central region, maintaining the rank association for nonoutliers, and detecting correct outliers for the above models. In Section 2, we first recall the definitions of global multivariate functional integrated depth (GMFID) and global multivariate functional extremal depth (GMFED), respectively. Then we show the proofs of Theorems 1-3.

¹Statistics Program, King Abdullah University of Science and Technology, Thuwal 23955-6900, Saudi Arabia.
E-mail: zhuo.qu@kaust.edu.sa, marc.genton@kaust.edu.sa

This research was supported by the King Abdullah University of Science and Technology (KAUST).

²Institute of Statistics and Big Data, Renmin University of China, Beijing 100872, China.
E-mail: wenlin.dai@ma.ma.cn

1 Simulation Study

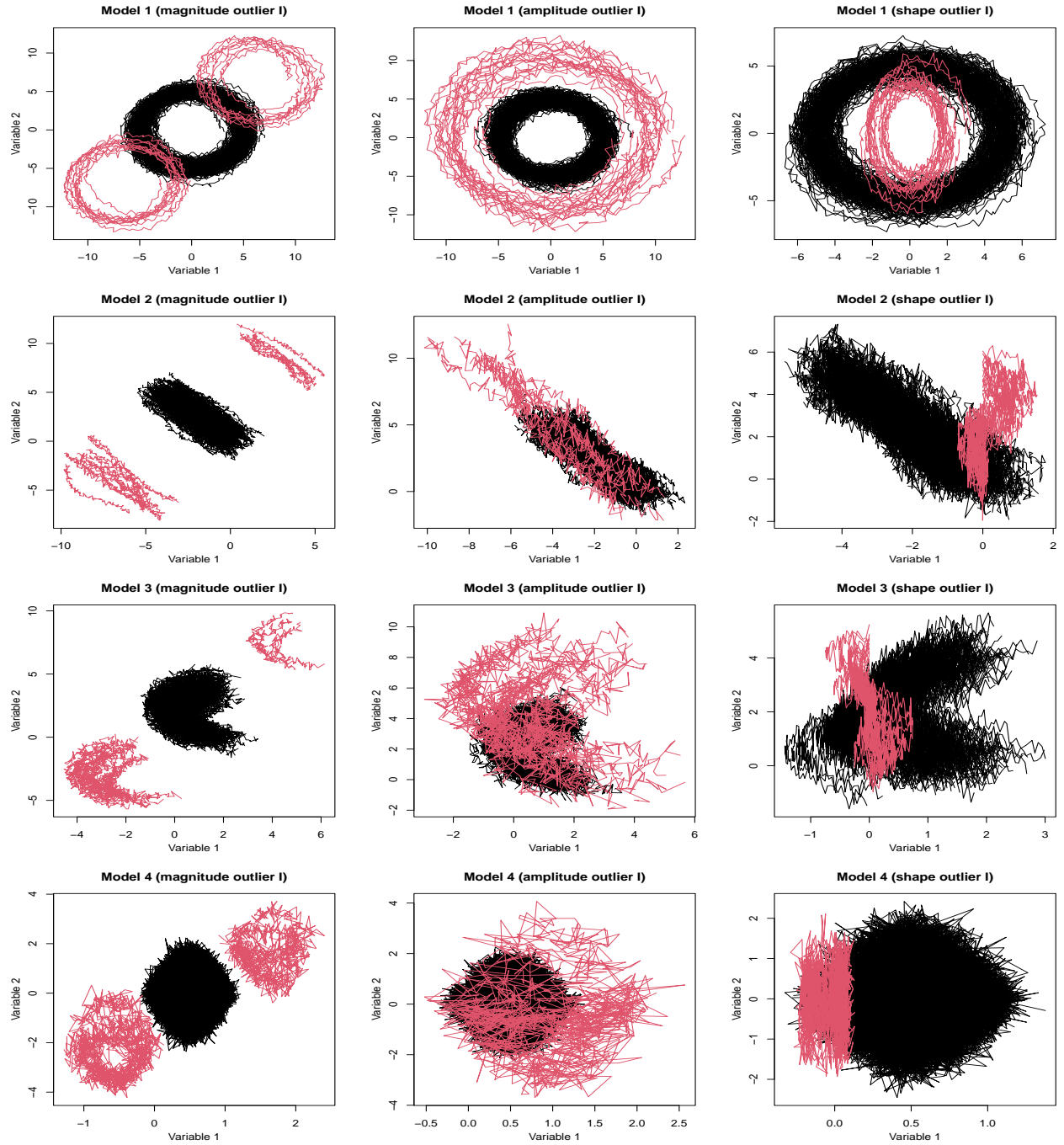


Figure S1: Panels from top to bottom show Models 1-4 contaminated by different types of outliers. Each panel displays the model contaminated by a 10% proportion of magnitude outlier I, amplitude outlier I, and shape outlier I, respectively, from left to right. The non-outlying and outlying curves are colored in black and red, respectively.

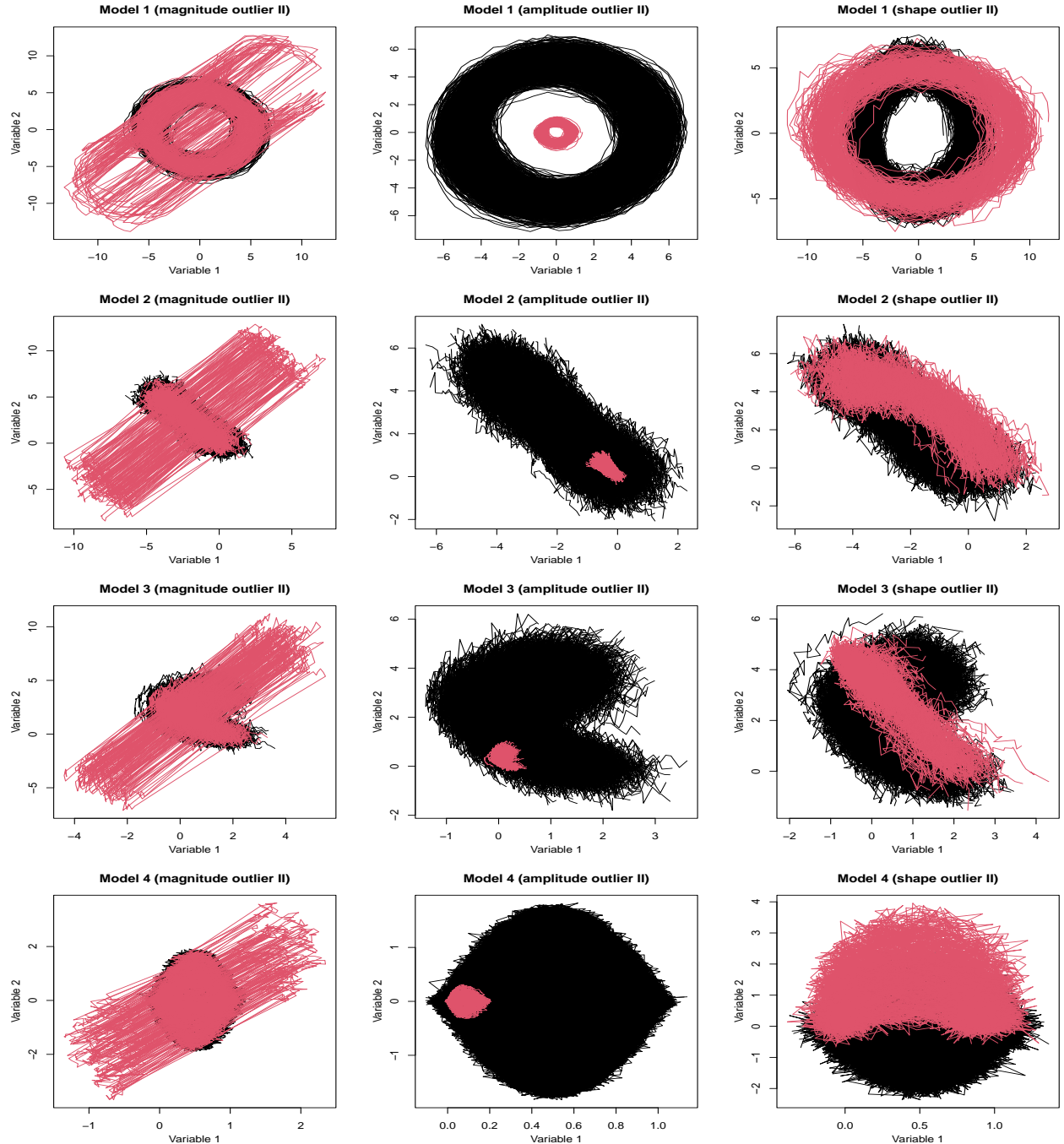


Figure S2: Panels from top to bottom show Models 1-4 contaminated by different types of outliers. Each panel displays the model contaminated by a 10% proportion of magnitude outlier II, amplitude outlier II, and shape outlier II, respectively, from left to right. The non-outlying and outlying curves are colored in black and red, respectively.

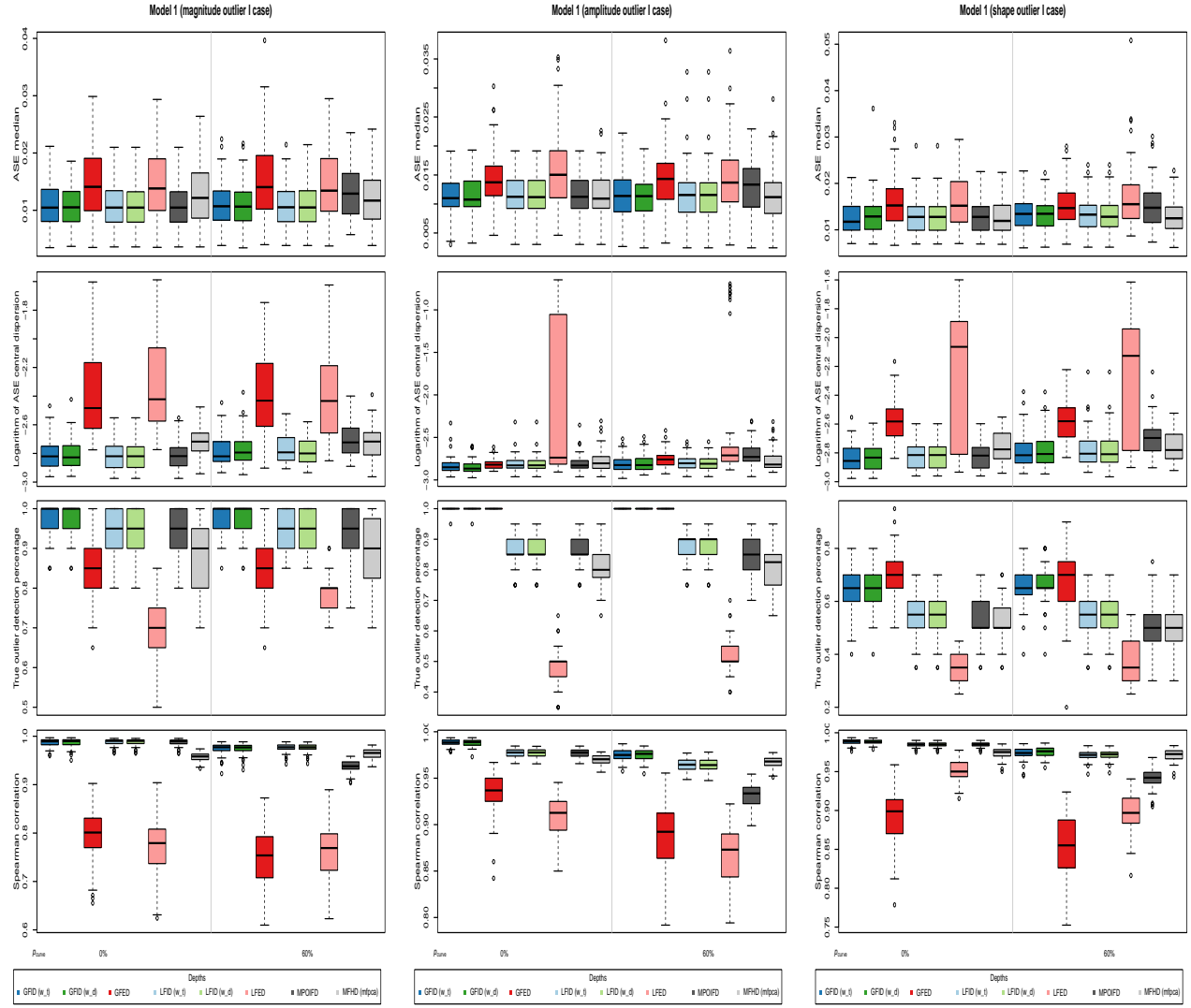


Figure S3: Left column shows Model 1 with magnitude outlier I, the middle column shows Model 1 with amplitude outlier I, and the right column shows Model 1 with shape outlier I. ASE of the estimated central curve (the first row), ASE of the 50%-dispersion curve (the second row), the outlier proportion in the lowest 10% depth region (the third row), and Spearman correlation (the fourth row). The sparseness type is **point** sparseness with a dense case ($p_{curve} = 0\%$) and a high sparseness case ($p_{curve} \sim \mathcal{U}(0.4, 0.6)$).

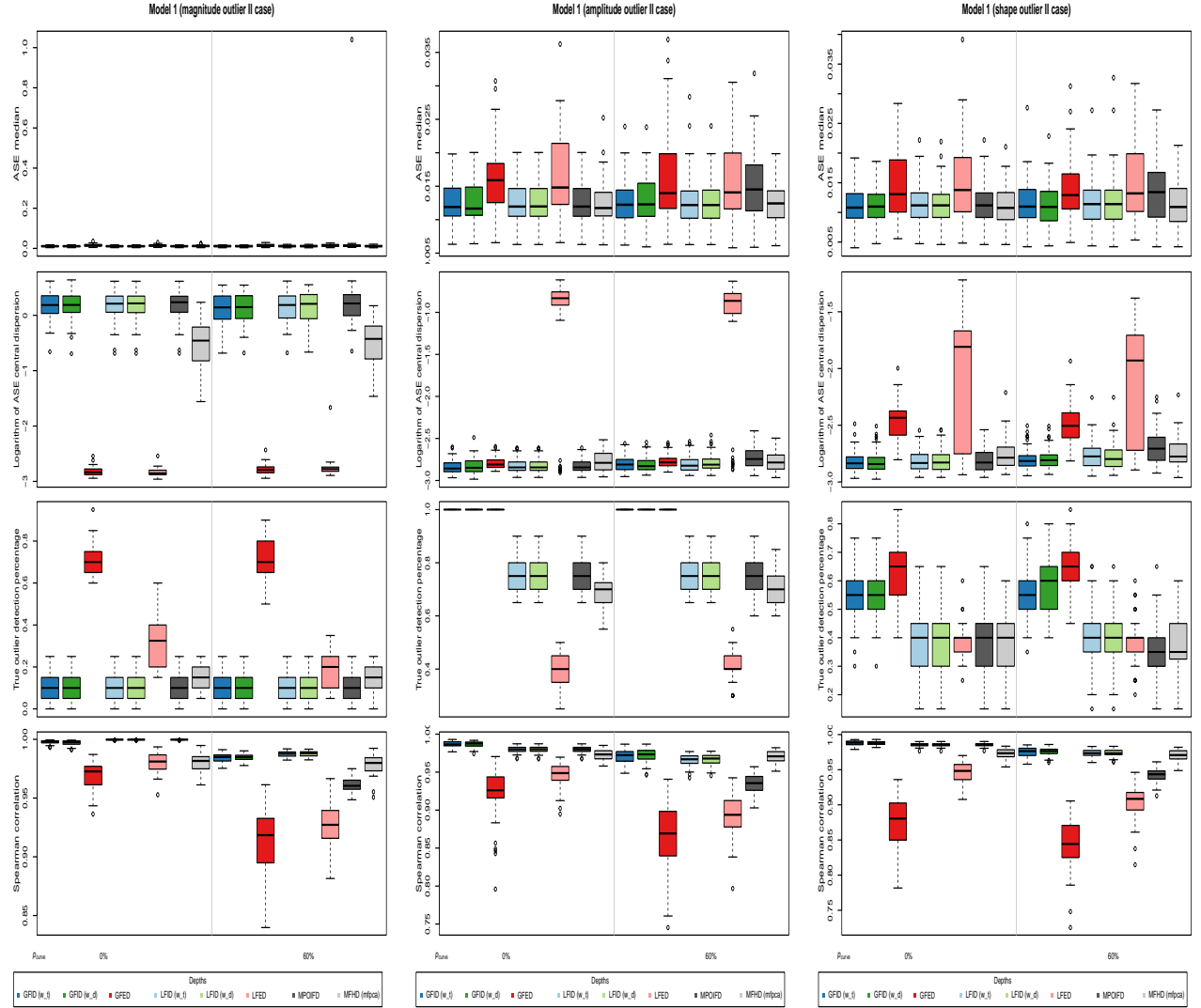


Figure S4: Left column shows Model 1 with magnitude outlier II, the middle column shows Model 1 with amplitude outlier II, and the right column shows Model 1 with shape outlier II. ASE of the estimated central curve (the first row), ASE of the 50%-dispersion curve (the second row), the outlier proportion in the lowest 10% depth region (the third row), and Spearman correlation (the fourth row). The sparseness type is **point** sparseness with a dense case ($p_{curve} = 0\%$) and a high sparseness case ($p_{curve} \sim \mathcal{U}(0.4, 0.6)$).

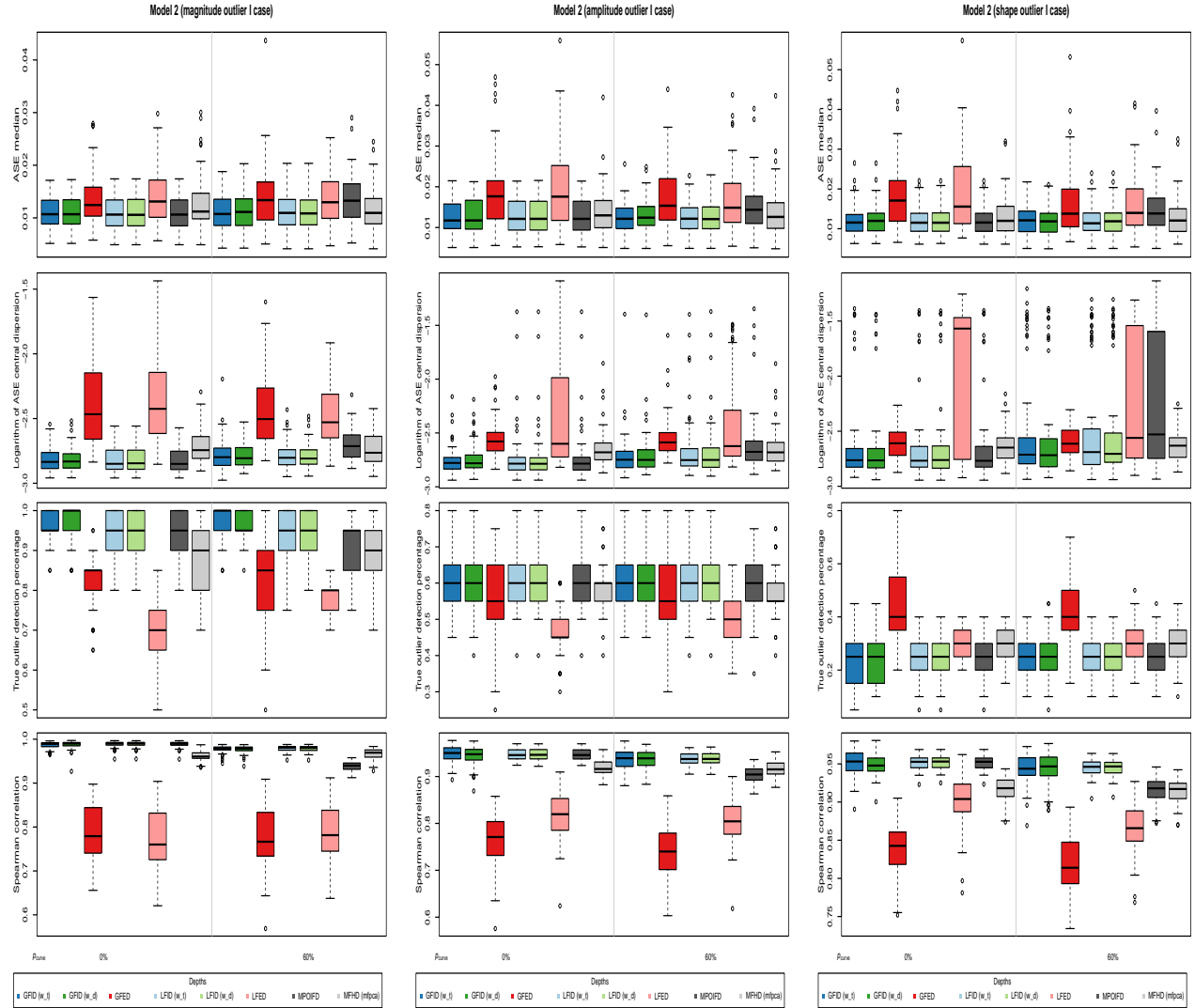


Figure S5: Left column shows Model 2 with magnitude outlier I, the middle column shows Model 2 with amplitude outlier I, and the right column shows Model 2 with shape outlier I. ASE of the estimated central curve (the first row), ASE of the 50%-dispersion curve (the second row), the outlier proportion in the lowest 10% depth region (the third row), and Spearman correlation (the fourth row). The sparseness type is **point** sparseness with a dense case ($p_{curve} = 0\%$) and a high sparseness case ($p_{curve} \sim \mathcal{U}(0.4, 0.6)$).

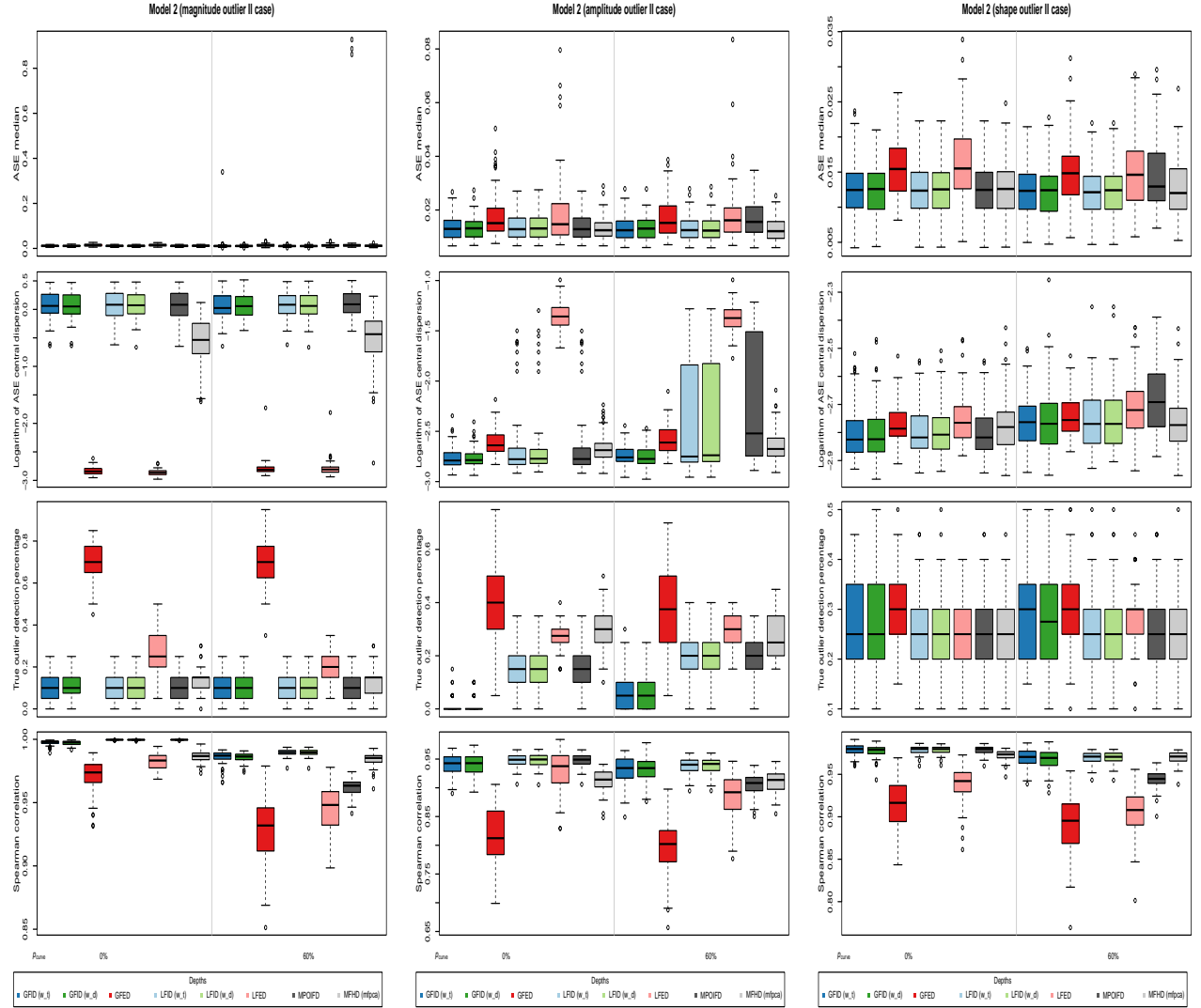


Figure S6: Left column shows Model 2 with magnitude outlier II, the middle column shows Model 2 with amplitude outlier II, and the right column shows Model 2 with shape outlier II. ASE of the estimated central curve (the first row), ASE of the 50%-dispersion curve (the second row), the outlier proportion in the lowest 10% depth region (the third row), and Spearman correlation (the fourth row). The sparseness type is **point** sparseness with a dense case ($p_{curve} = 0\%$) and a high sparseness case ($p_{curve} \sim \mathcal{U}(0.4, 0.6)$).

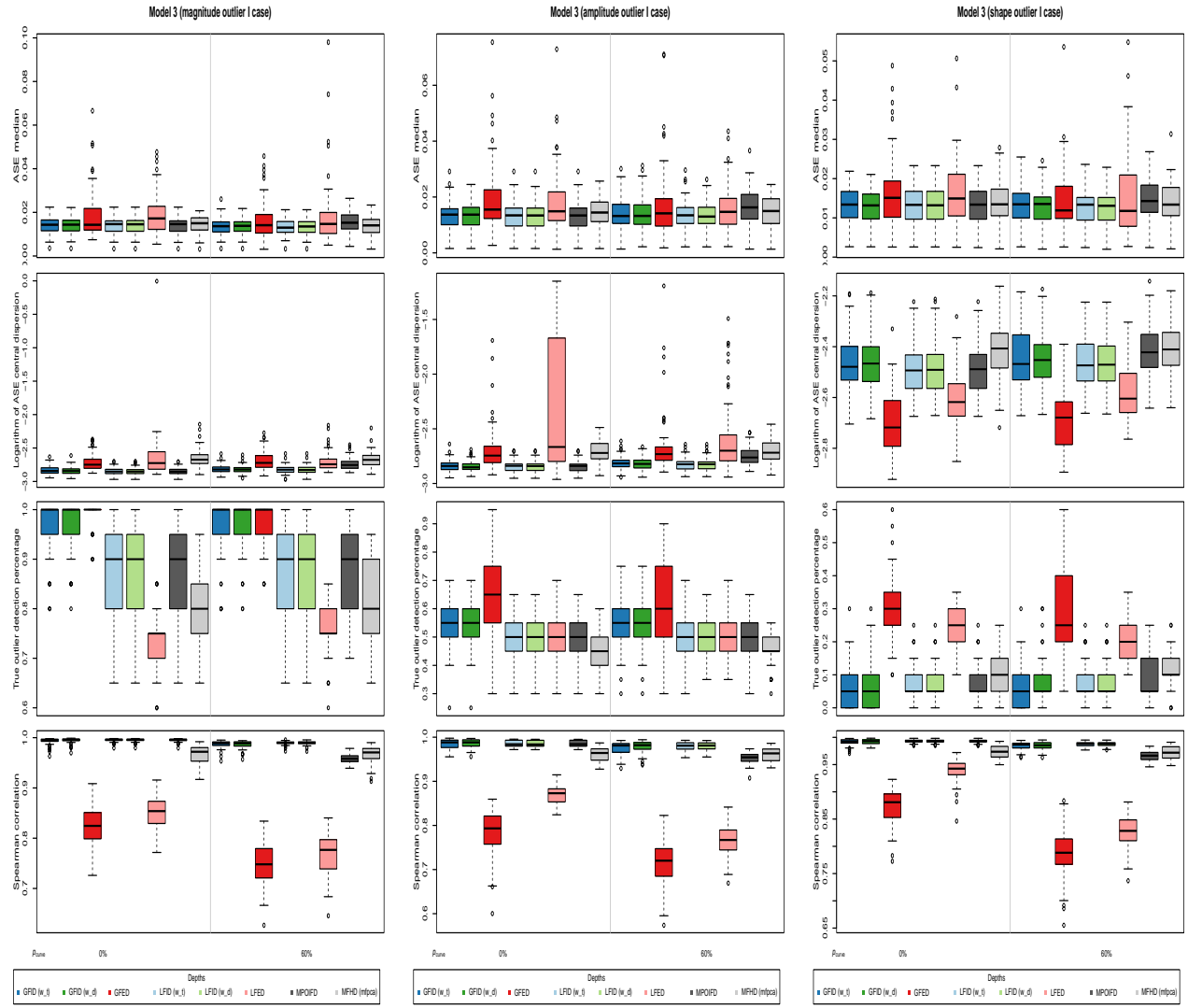


Figure S7: Left column shows Model 3 with magnitude outlier I, the middle column shows Model 3 with amplitude outlier I, and the right column shows Model 3 with shape outlier I. ASE of the estimated central curve (the first row), ASE of the 50%-dispersion curve (the second row), the outlier proportion in the lowest 10% depth region (the third row), and Spearman correlation (the fourth row). The sparseness type is **point** sparseness with a dense case ($p_{curve} = 0\%$) and a high sparseness case ($p_{curve} \sim \mathcal{U}(0.4, 0.6)$).

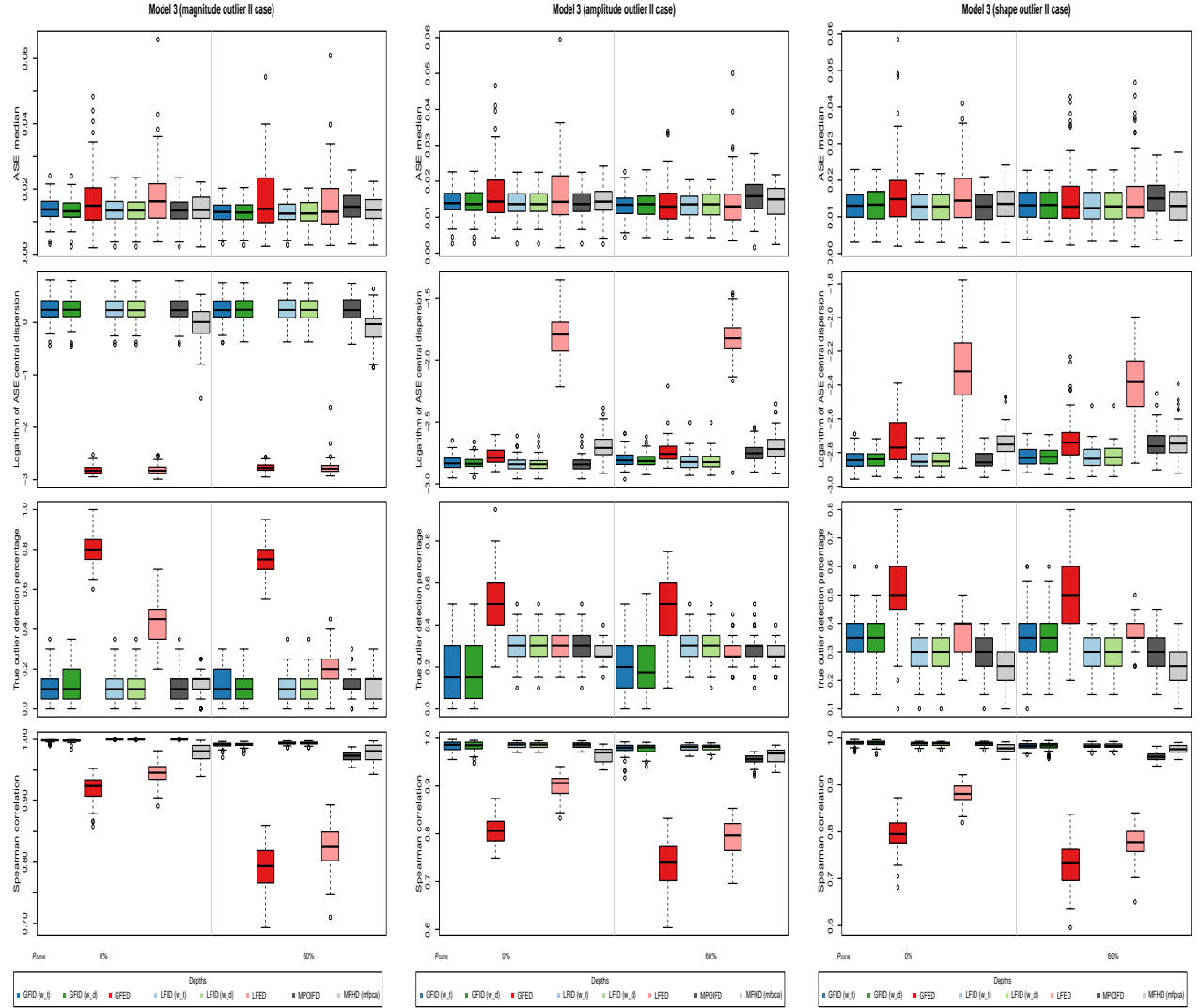


Figure S8: Left column shows Model 3 with magnitude outlier II, the middle column shows Model 3 with amplitude outlier II, and the right column shows Model 3 with shape outlier II. ASE of the estimated central curve (the first row), ASE of the 50%-dispersion curve (the second row), the outlier proportion in the lowest 10% depth region (the third row), and Spearman correlation (the fourth row). The sparseness type is **point** sparseness with a dense case ($p_{curve} = 0\%$) and a high sparseness case ($p_{curve} \sim \mathcal{U}(0.4, 0.6)$).

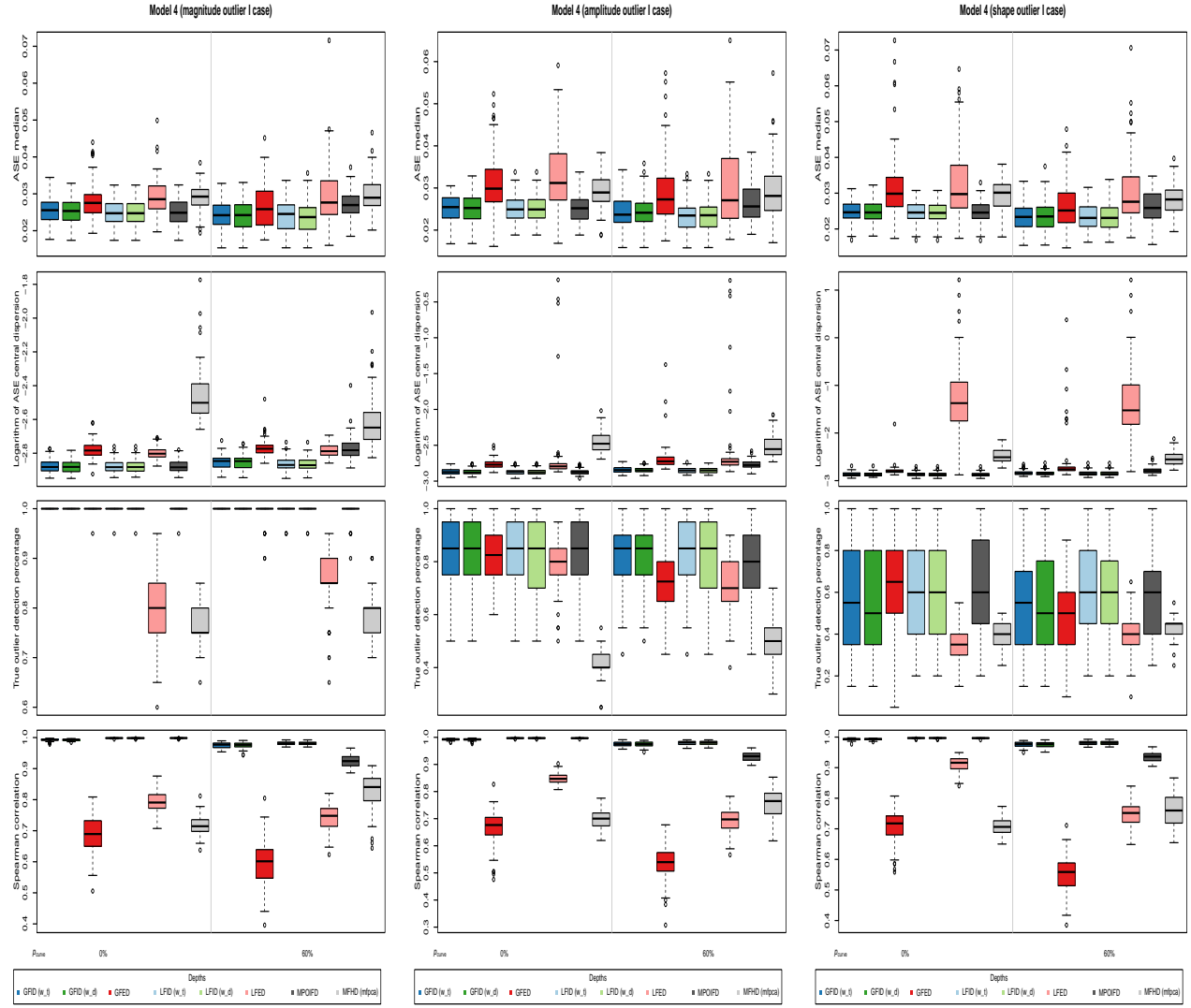


Figure S9: Left column shows Model 4 with magnitude outlier I, the middle column shows Model 4 with amplitude outlier I, and the right column shows Model 4 with shape outlier I. ASE of the estimated central curve (the first row), ASE of the 50%-dispersion curve (the second row), the outlier proportion in the lowest 10% depth region (the third row), and Spearman correlation (the fourth row). The sparseness type is **point** sparseness with a dense case ($p_{curve} = 0\%$) and a high sparseness case ($p_{curve} \sim \mathcal{U}(0.4, 0.6)$).

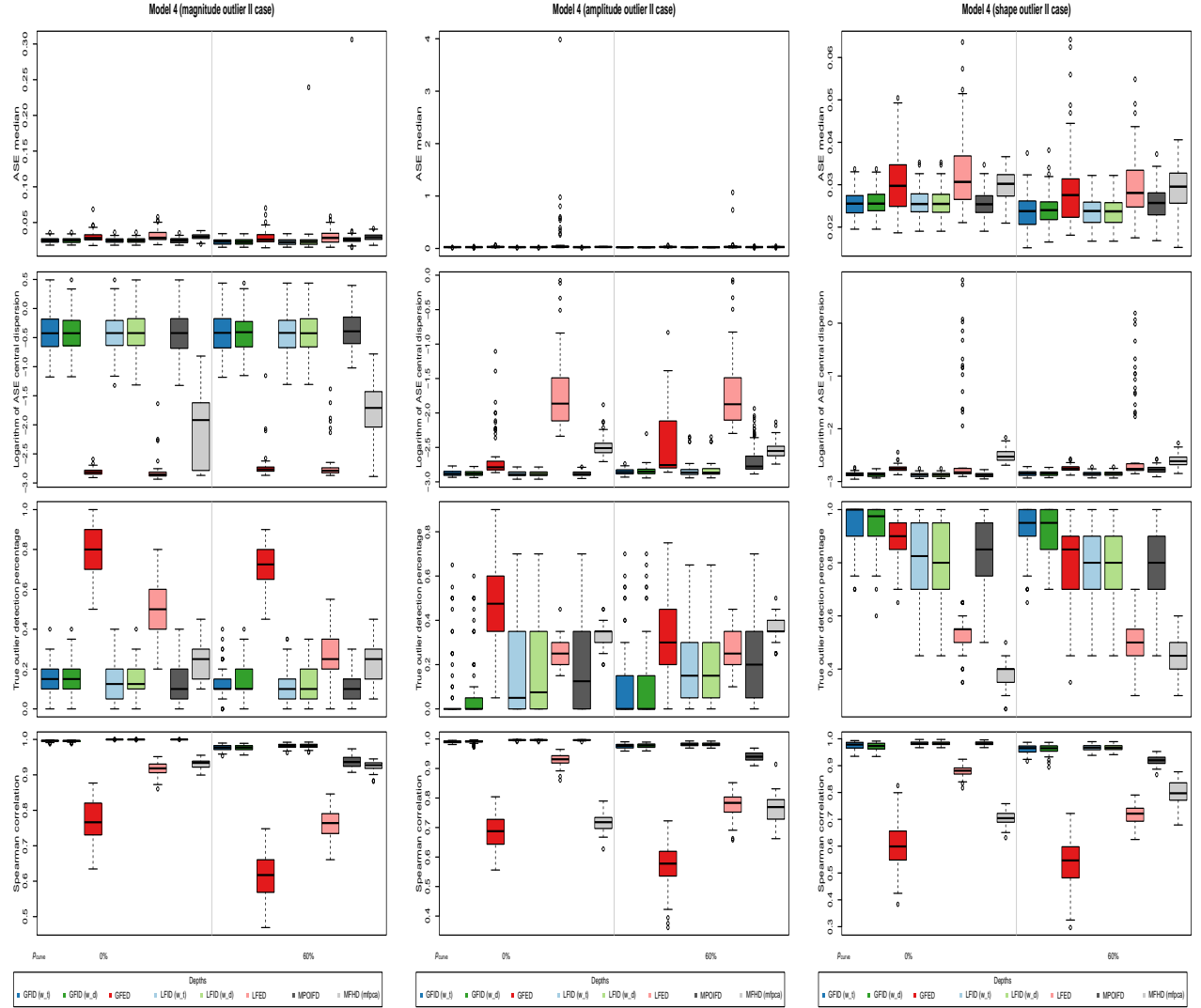


Figure S10: Left column shows Model 4 with magnitude outlier II, the middle column shows Model 4 with amplitude outlier II, and the right column shows Model 4 with shape outlier II. ASE of the estimated central curve (the first row), ASE of the 50%-dispersion curve (the second row), the outlier proportion in the lowest 10% depth region (the third row), and Spearman correlation (the fourth row). The sparseness type is **point** sparseness with a dense case ($p_{curve} = 0\%$) and a high sparseness case ($p_{curve} \sim \mathcal{U}(0.4, 0.6)$).

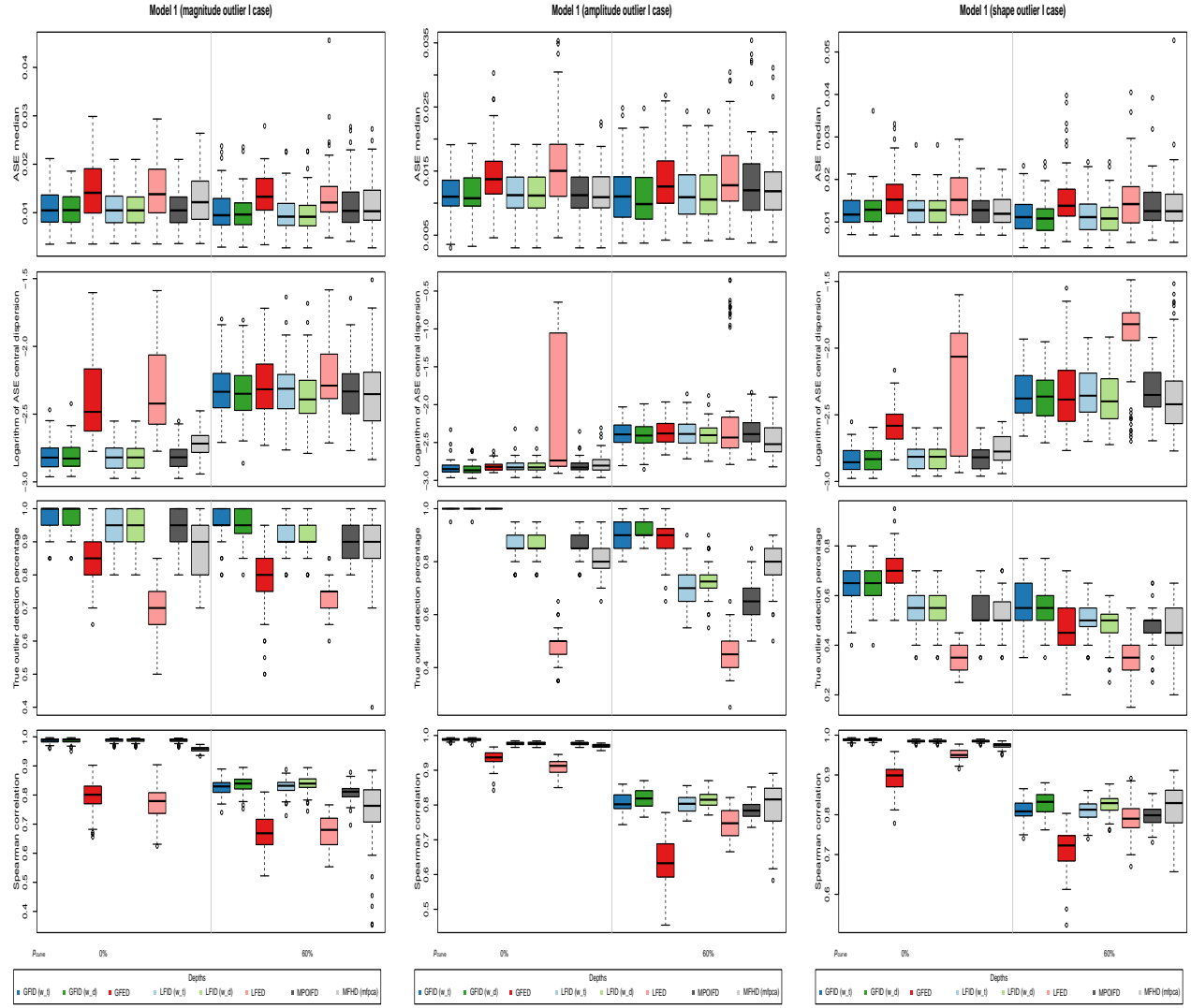


Figure S11: Left column shows Model 1 with magnitude outlier I, the middle column shows Model 1 with amplitude outlier I, and the right column shows Model 1 with shape outlier I. ASE of the estimated central curve (the first row), ASE of the 50%-dispersion curve (the second row), the outlier proportion in the lowest 10% depth region (the third row), and Spearman correlation (the fourth row). The sparseness type is peak sparseness with a dense case ($p_{curve} = 0\%$) and a high sparseness case ($p_{curve} \sim \mathcal{U}(0.4, 0.6)$).

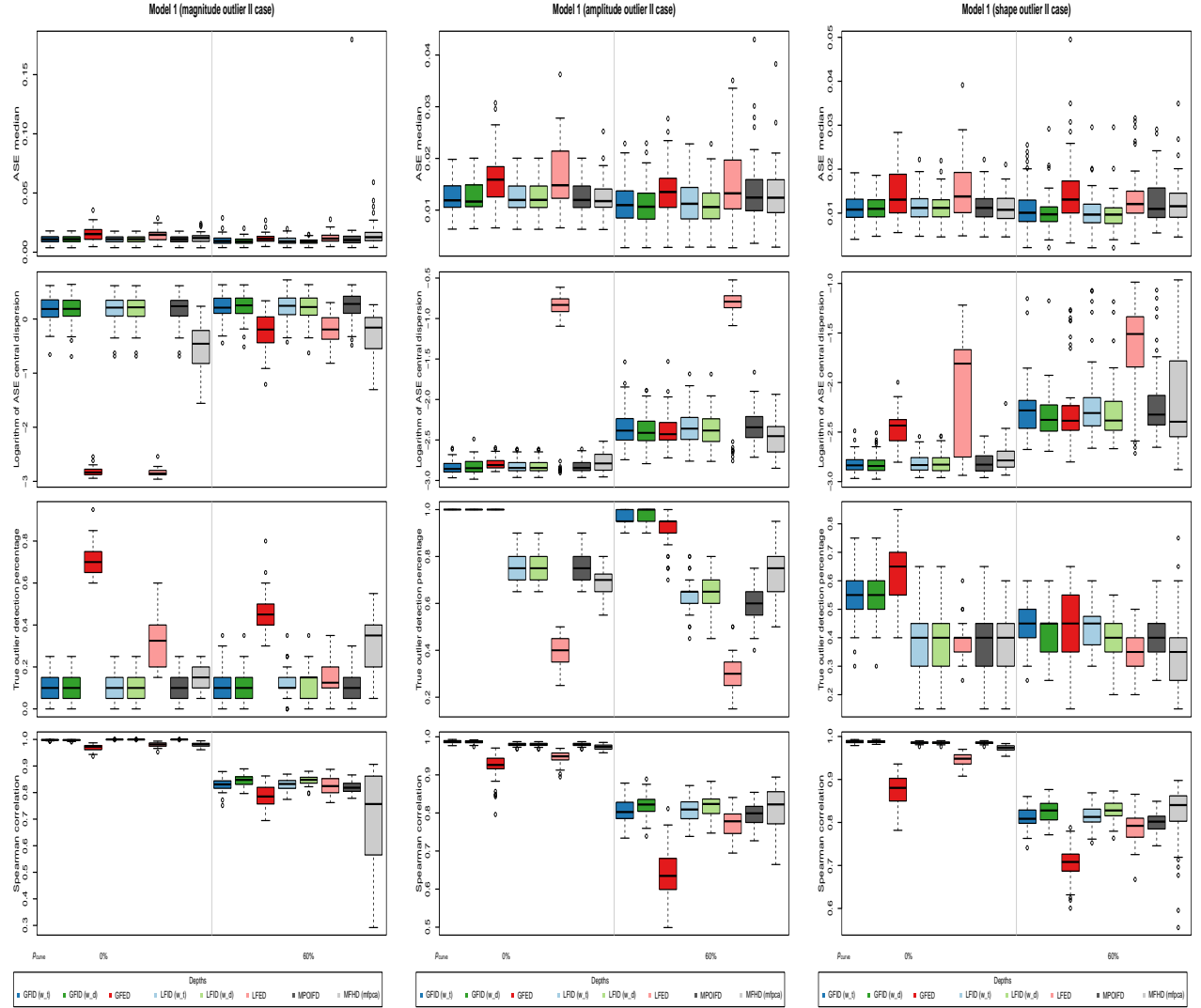


Figure S12: Left column shows Model 1 with magnitude outlier II, the middle column shows Model 1 with amplitude outlier II, and the right column shows Model 1 with shape outlier II. ASE of the estimated central curve (the first row), ASE of the 50%-dispersion curve (the second row), the outlier proportion in the lowest 10% depth region (the third row), and Spearman correlation (the fourth row). The sparseness type is **peak** sparseness with a dense case ($p_{curve} = 0\%$) and a high sparseness case ($p_{curve} \sim \mathcal{U}(0.4, 0.6)$).

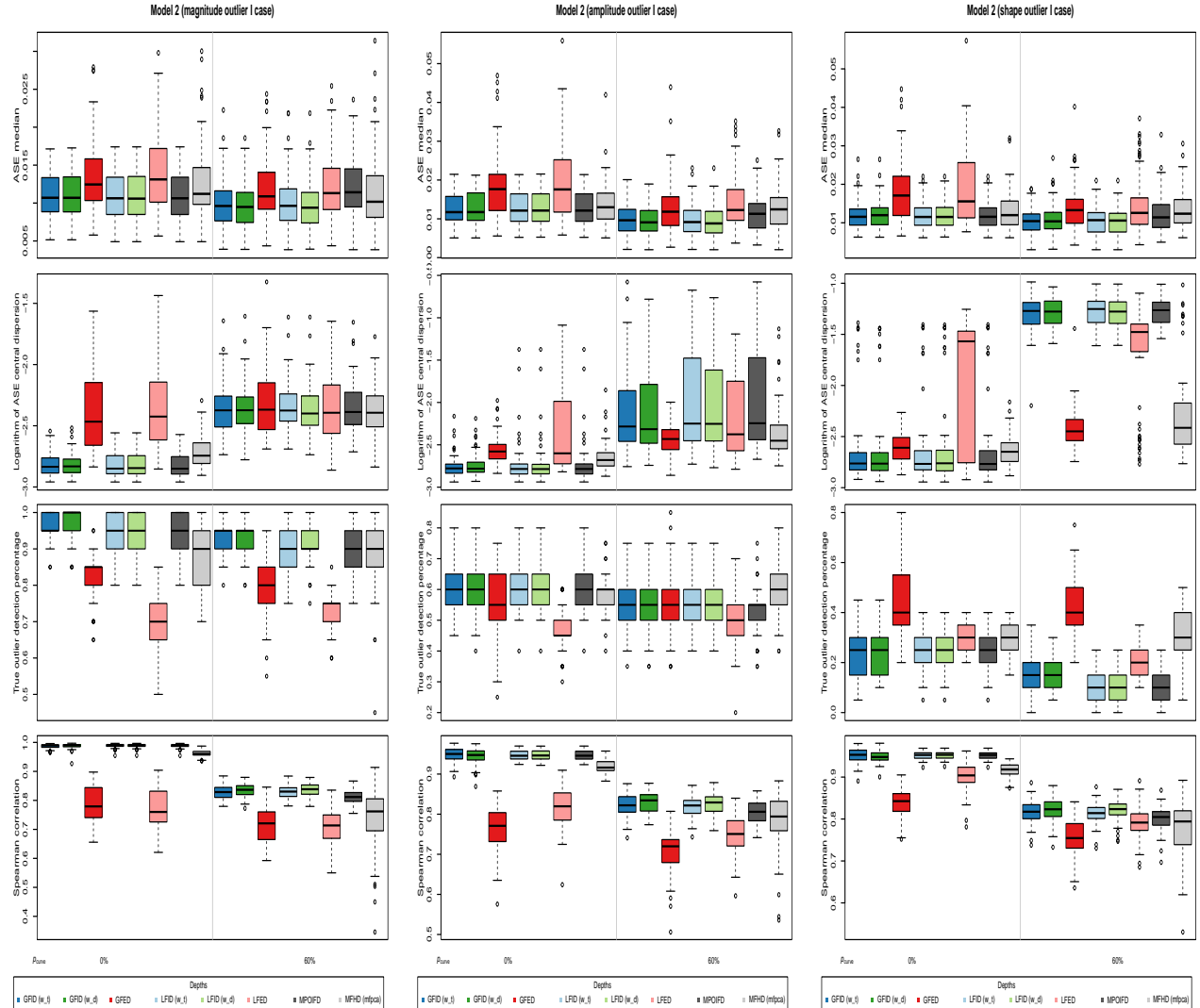


Figure S13: Left column shows Model 2 with magnitude outlier I, the middle column shows Model 2 with amplitude outlier I, and the right column shows Model 2 with shape outlier I. ASE of the estimated central curve (the first row), ASE of the 50%-dispersion curve (the second row), the outlier proportion in the lowest 10% depth region (the third row), and Spearman correlation (the fourth row). The sparseness type is **peak** sparseness with a dense case ($p_{curve} = 0\%$) and a high sparseness case ($p_{curve} \sim \mathcal{U}(0.4, 0.6)$).

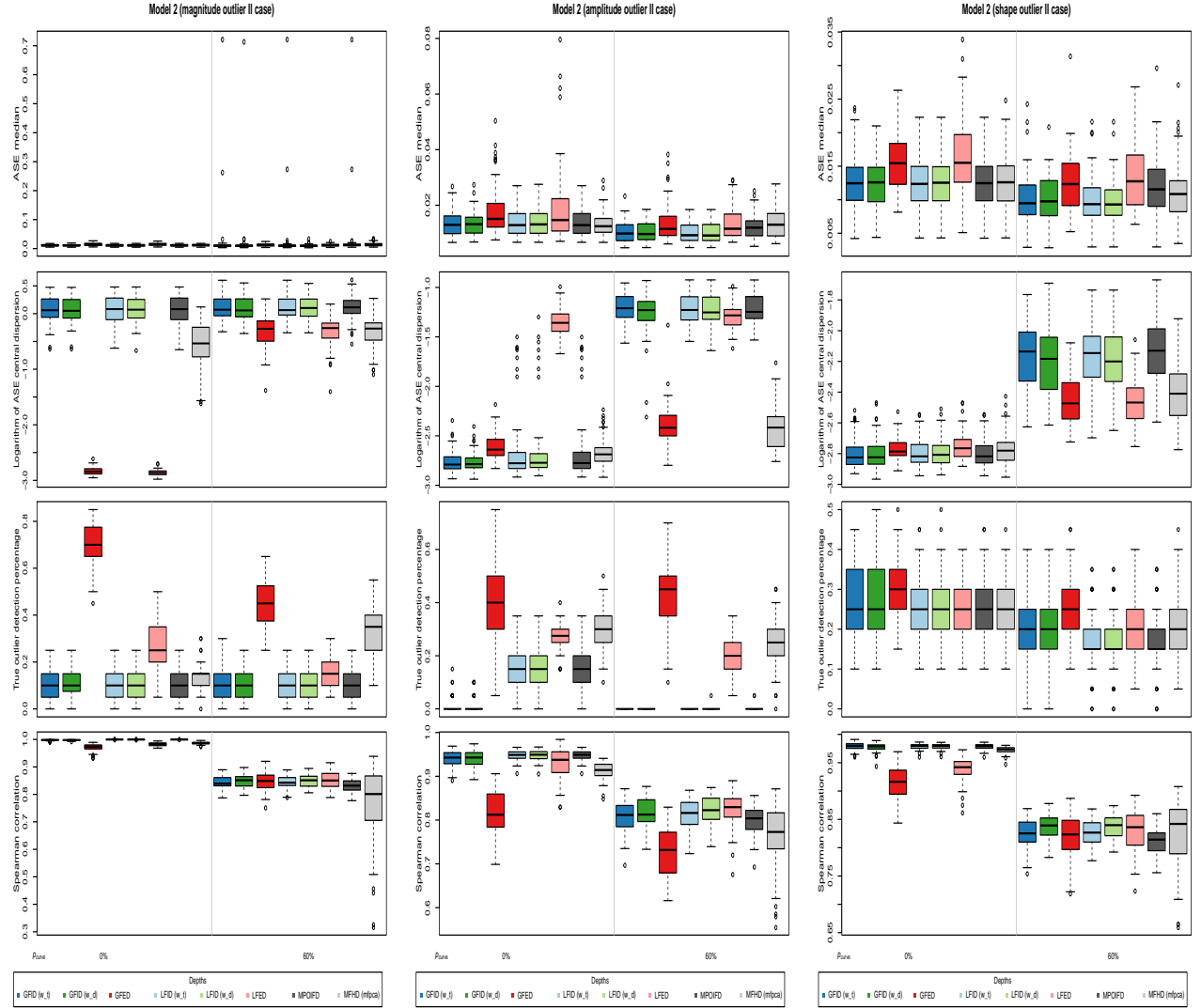


Figure S14: Left column shows Model 2 with magnitude outlier II, the middle column shows Model 2 with amplitude outlier II, and the right column shows Model 2 with shape outlier II. ASE of the estimated central curve (the first row), ASE of the 50%-dispersion curve (the second row), the outlier proportion in the lowest 10% depth region (the third row), and Spearman correlation (the fourth row). The sparseness type is **peak** sparseness with a dense case ($p_{curve} = 0\%$) and a high sparseness case ($p_{curve} \sim \mathcal{U}(0.4, 0.6)$).

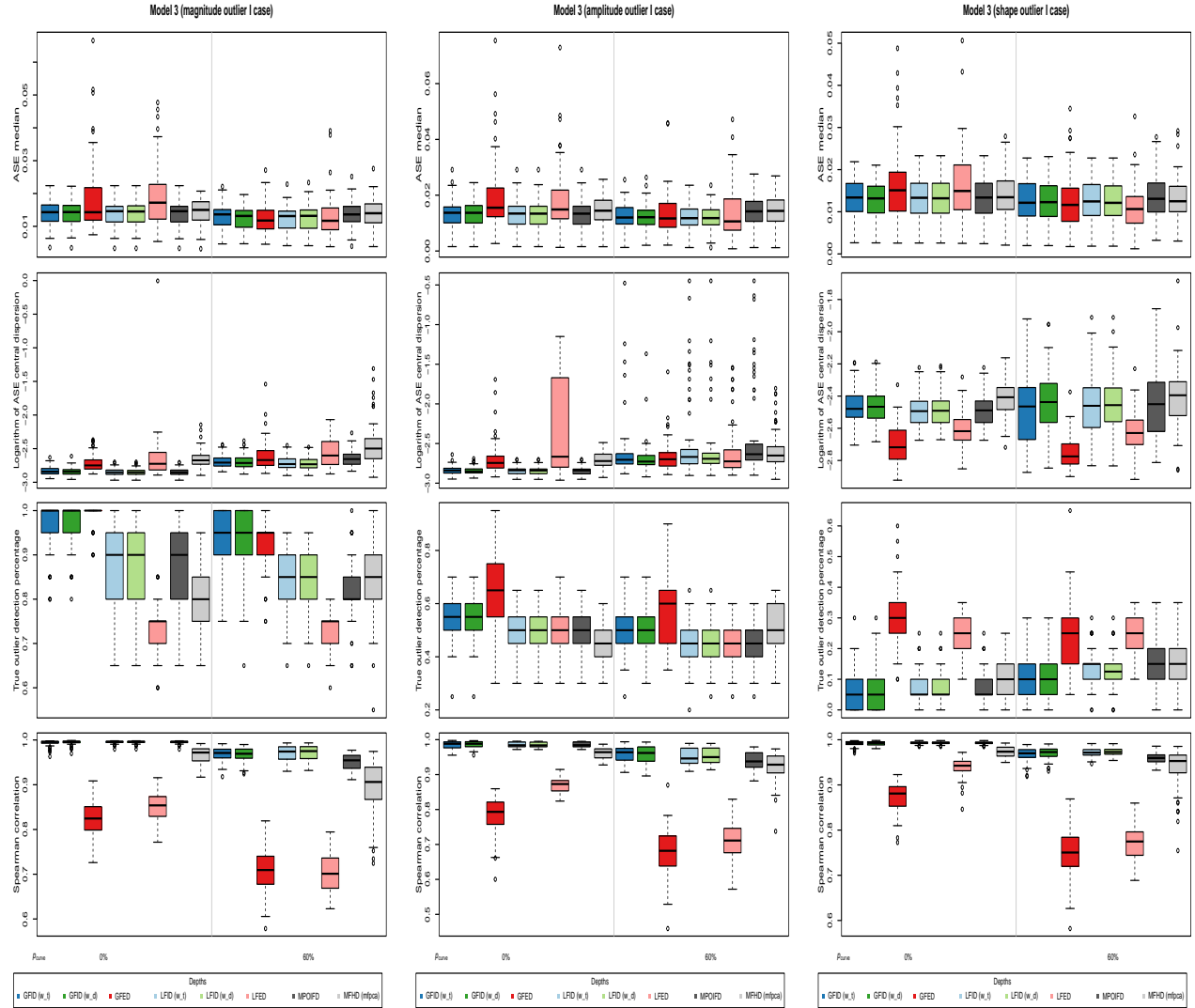


Figure S15: Left column shows Model 3 with magnitude outlier I, the middle column shows Model 3 with amplitude outlier I, and the right column shows Model 3 with shape outlier I. ASE of the estimated central curve (the first row), ASE of the 50%-dispersion curve (the second row), the outlier proportion in the lowest 10% depth region (the third row), and Spearman correlation (the fourth row). The sparseness type is **peak** sparseness with a dense case ($p_{curve} = 0\%$) and a high sparseness case ($p_{curve} \sim \mathcal{U}(0.4, 0.6)$).

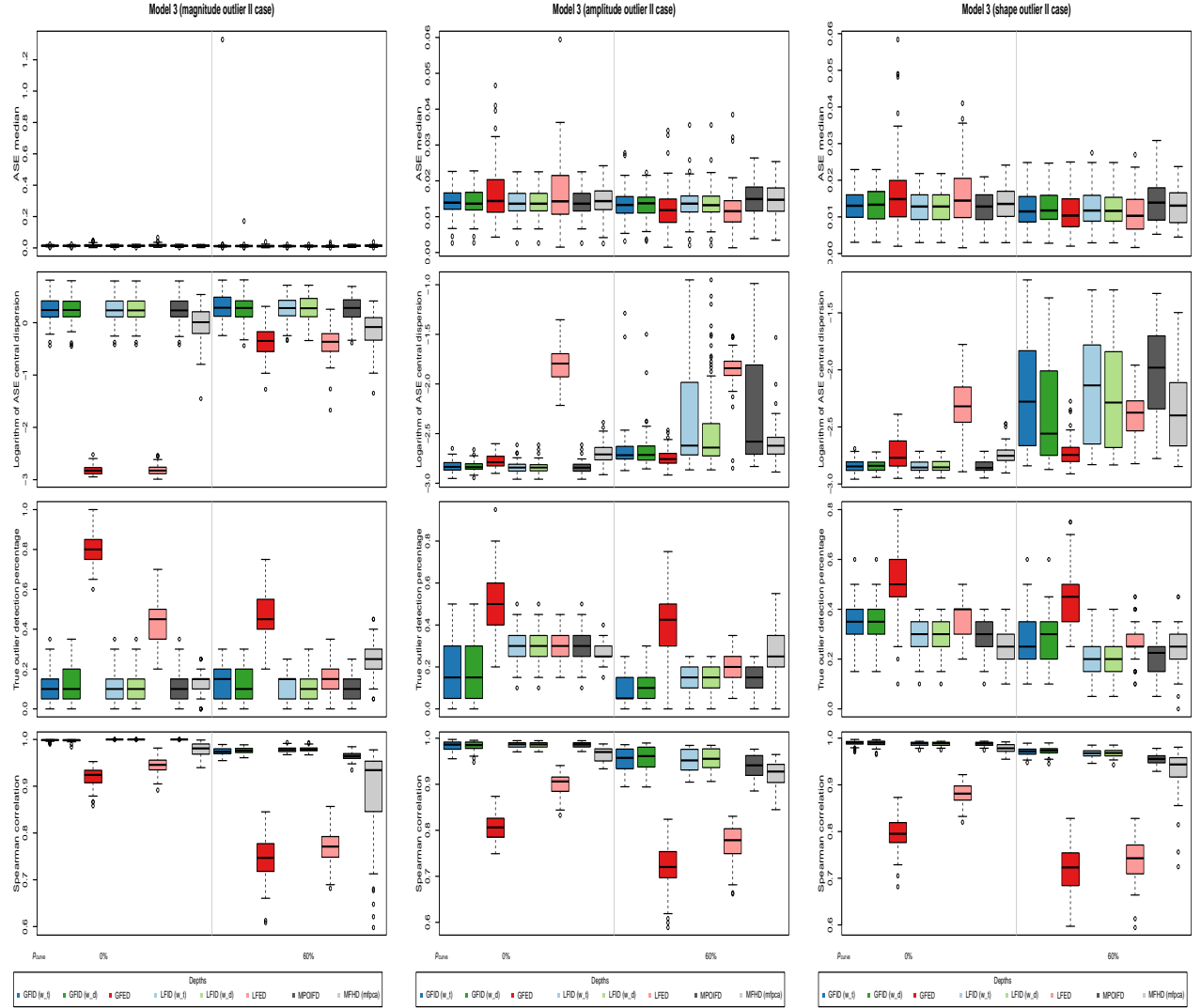


Figure S16: Left column shows Model 3 with magnitude outlier II, the middle column shows Model 3 with amplitude outlier II, and the right column shows Model 3 with shape outlier II. ASE of the estimated central curve (the first row), ASE of the 50%-dispersion curve (the second row), the outlier proportion in the lowest 10% depth region (the third row), and Spearman correlation (the fourth row). The sparseness type is **peak** sparseness with a dense case ($p_{curve} = 0\%$) and a high sparseness case ($p_{curve} \sim \mathcal{U}(0.4, 0.6)$).

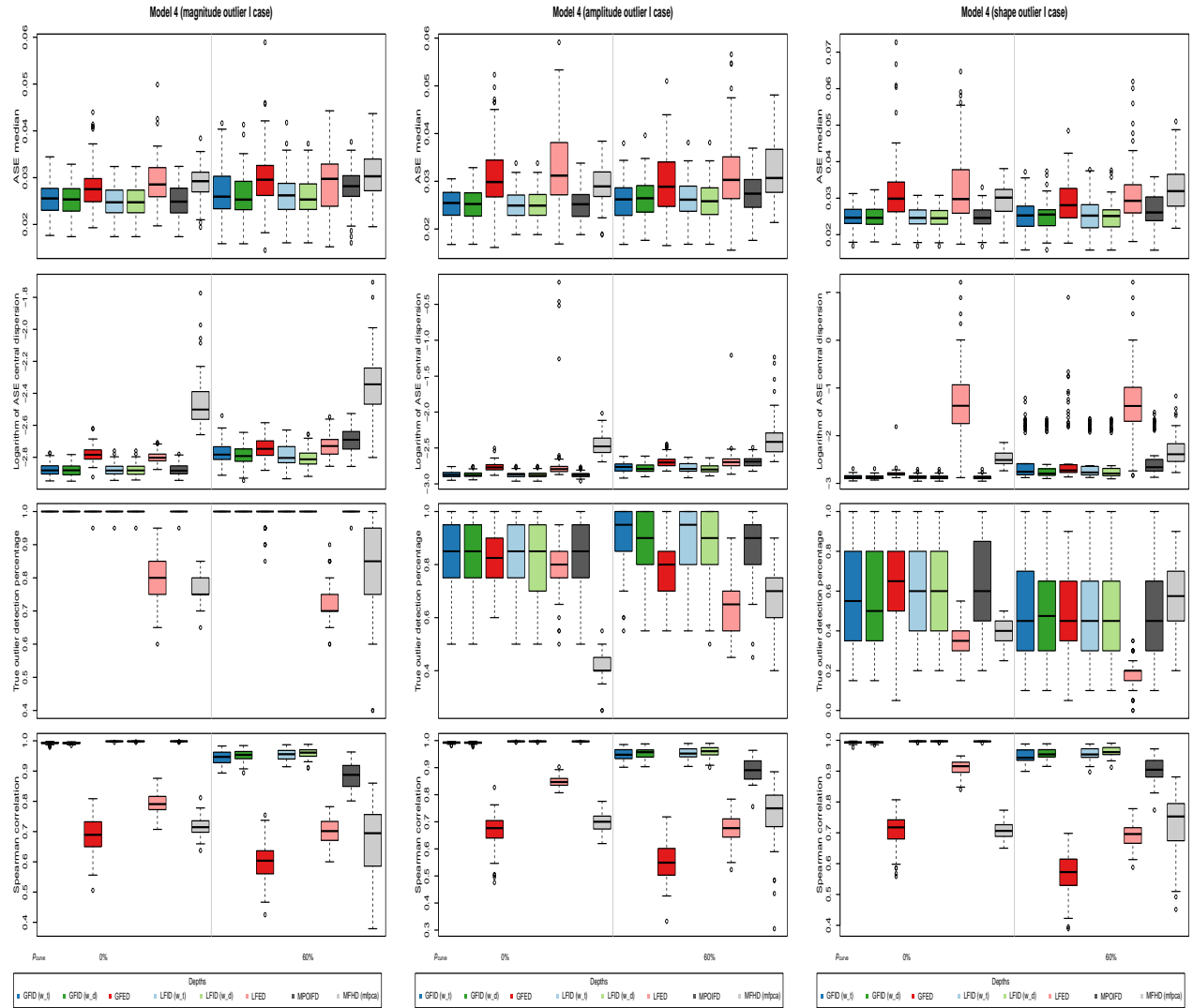


Figure S17: Left column shows Model 4 with magnitude outlier I, the middle column shows Model 4 with amplitude outlier I, and the right column shows Model 4 with shape outlier I. ASE of the estimated central curve (the first row), ASE of the 50%-dispersion curve (the second row), the outlier proportion in the lowest 10% depth region (the third row), and Spearman correlation (the fourth row). The sparseness type is **peak** sparseness with a dense case ($p_{curve} = 0\%$) and a high sparseness case ($p_{curve} \sim \mathcal{U}(0.4, 0.6)$).

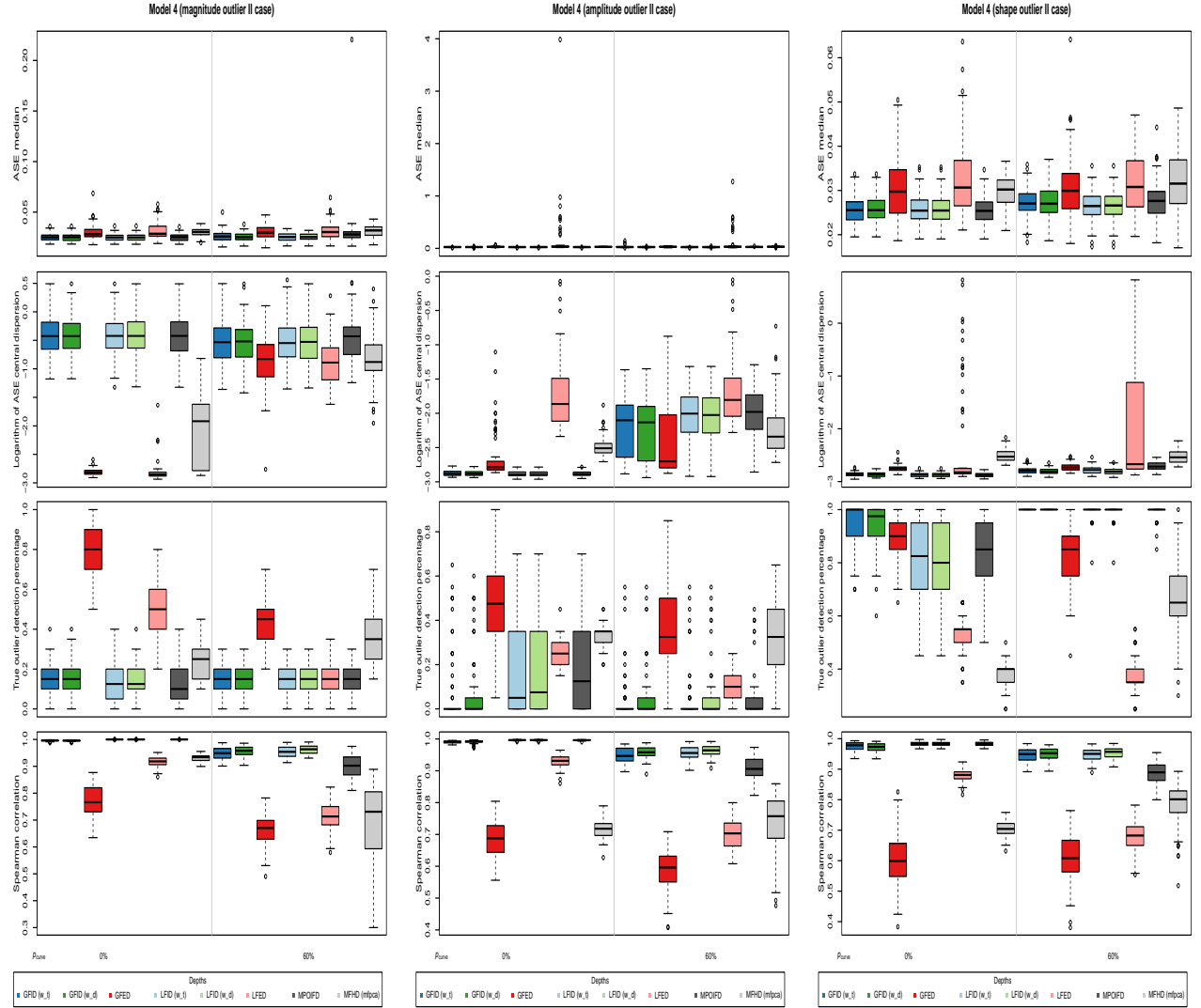


Figure S18: Left column shows Model 4 with magnitude outlier II, the middle column shows Model 4 with amplitude outlier II, and the right column shows Model 4 with shape outlier II. ASE of the estimated central curve (the first row), ASE of the 50%-dispersion curve (the second row), the outlier proportion in the lowest 10% depth region (the third row), and Spearman correlation (the fourth row). The sparseness type is **peak** sparseness with a dense case ($p_{curve} = 0\%$) and a high sparseness case ($p_{curve} \sim \mathcal{U}(0.4, 0.6)$).

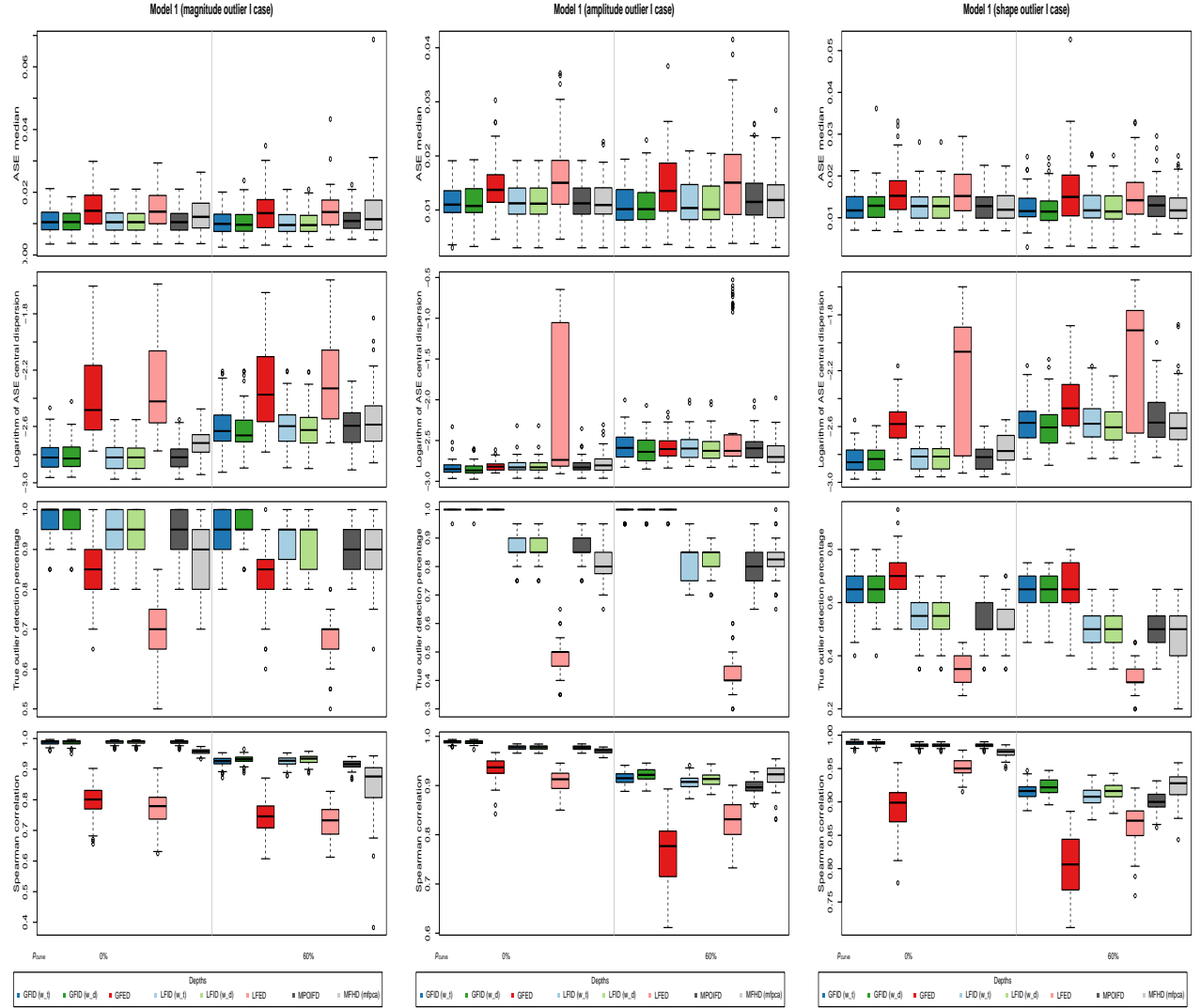


Figure S19: Left column shows Model 1 with magnitude outlier I, the middle column shows Model 1 with amplitude outlier I, and the right column shows Model 1 with shape outlier I. ASE of the estimated central curve (the first row), ASE of the 50%-dispersion curve (the second row), the outlier proportion in the lowest 10% depth region (the third row), and Spearman correlation (the fourth row). The sparseness type is partial sparseness with a dense case ($p_{curve} = 0\%$) and a high sparseness case ($p_{curve} \sim \mathcal{U}(0.4, 0.6)$).

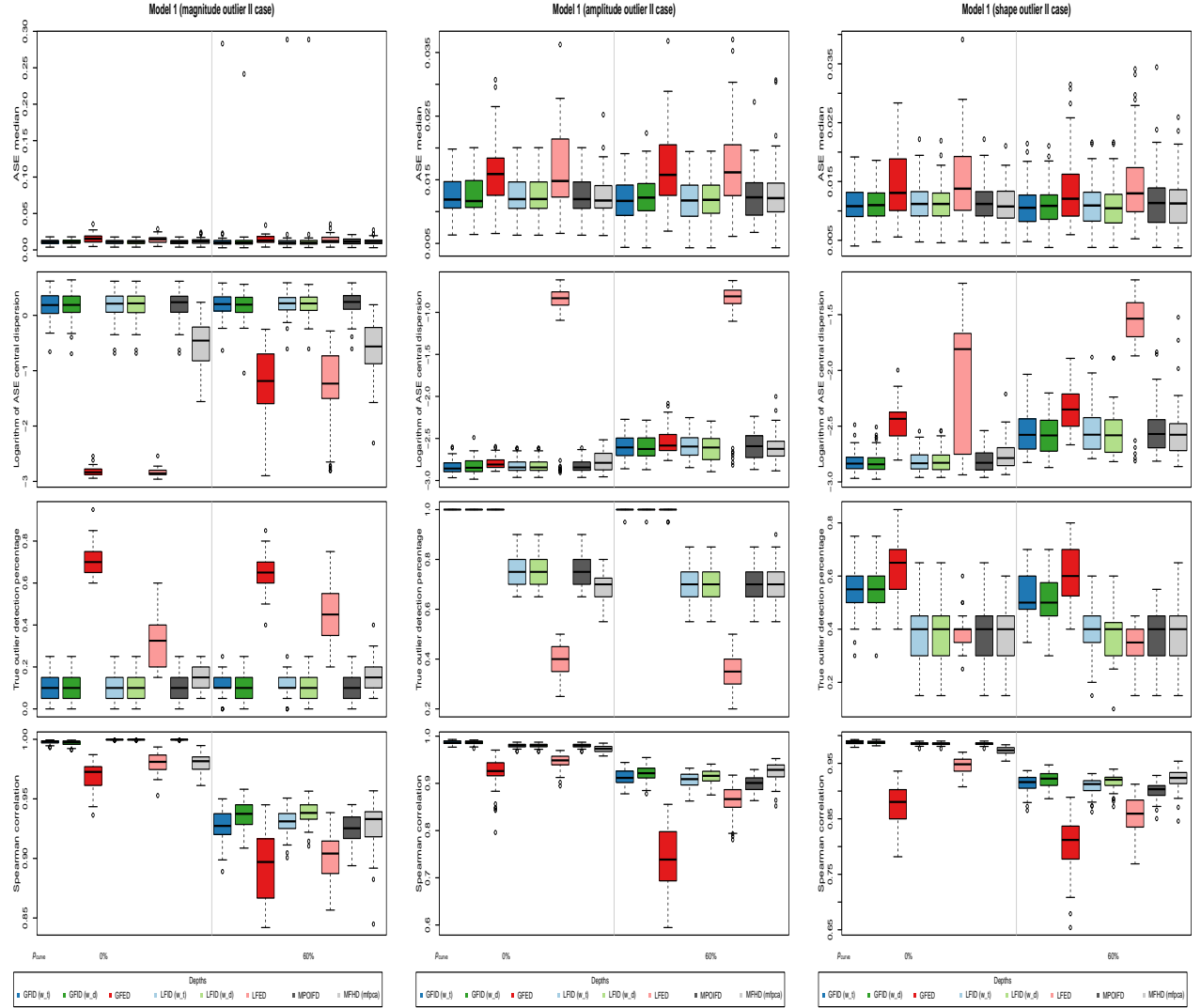


Figure S20: Left column shows Model 1 with magnitude outlier II, the middle column shows Model 1 with amplitude outlier II, and the right column shows Model 1 with shape outlier II. ASE of the estimated central curve (the first row), ASE of the 50%-dispersion curve (the second row), the outlier proportion in the lowest 10% depth region (the third row), and Spearman correlation (the fourth row). The sparseness type is **partial** sparseness with a dense case ($p_{curve} = 0\%$) and a high sparseness case ($p_{curve} \sim \mathcal{U}(0.4, 0.6)$).

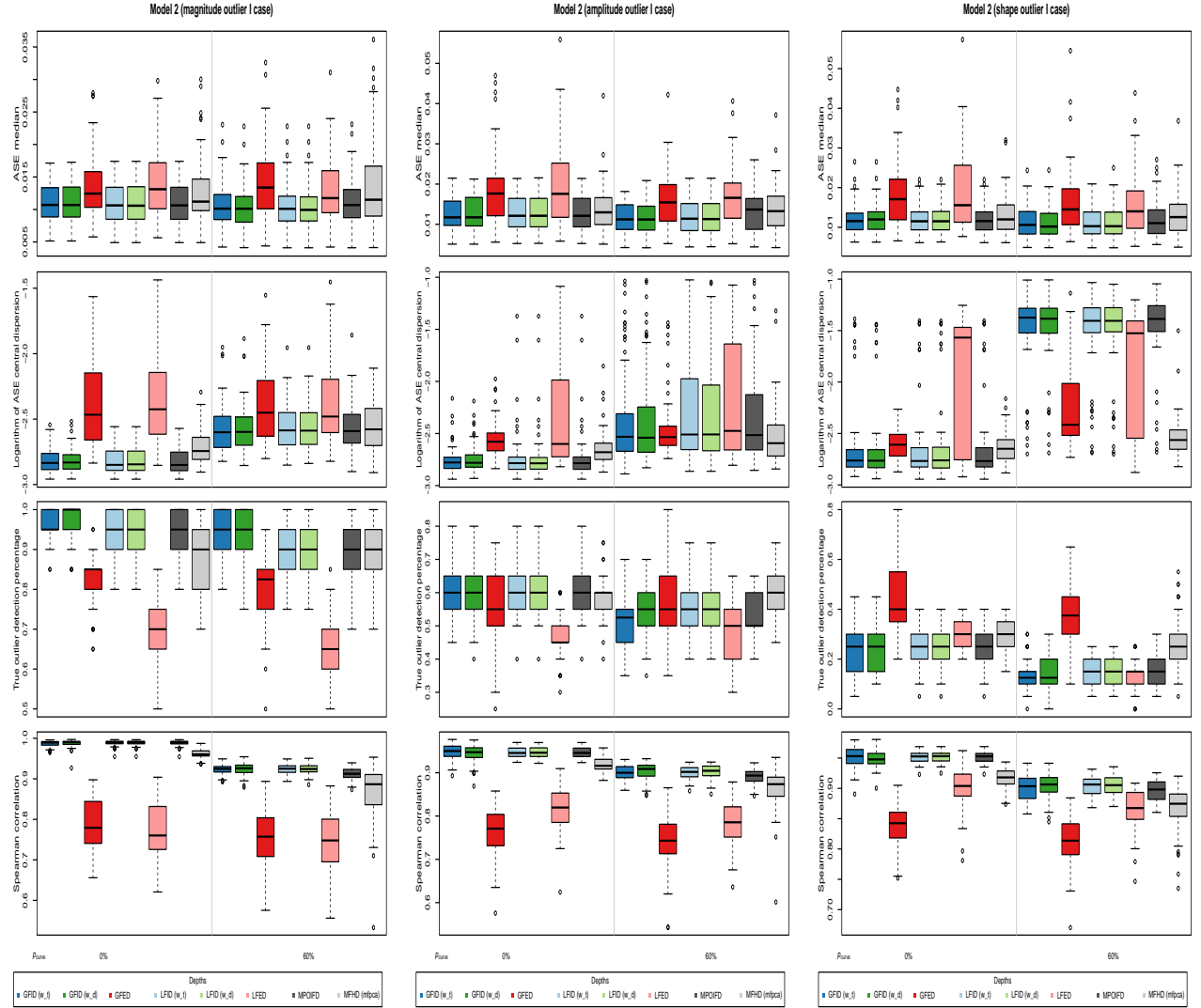


Figure S21: Left column shows Model 2 with magnitude outlier I, the middle column shows Model 2 with amplitude outlier I, and the right column shows Model 2 with shape outlier I. ASE of the estimated central curve (the first row), ASE of the 50%-dispersion curve (the second row), the outlier proportion in the lowest 10% depth region (the third row), and Spearman correlation (the fourth row). The sparseness type is **partial** sparseness with a dense case ($p_{curve} = 0\%$) and a high sparseness case ($p_{curve} \sim \mathcal{U}(0.4, 0.6)$).

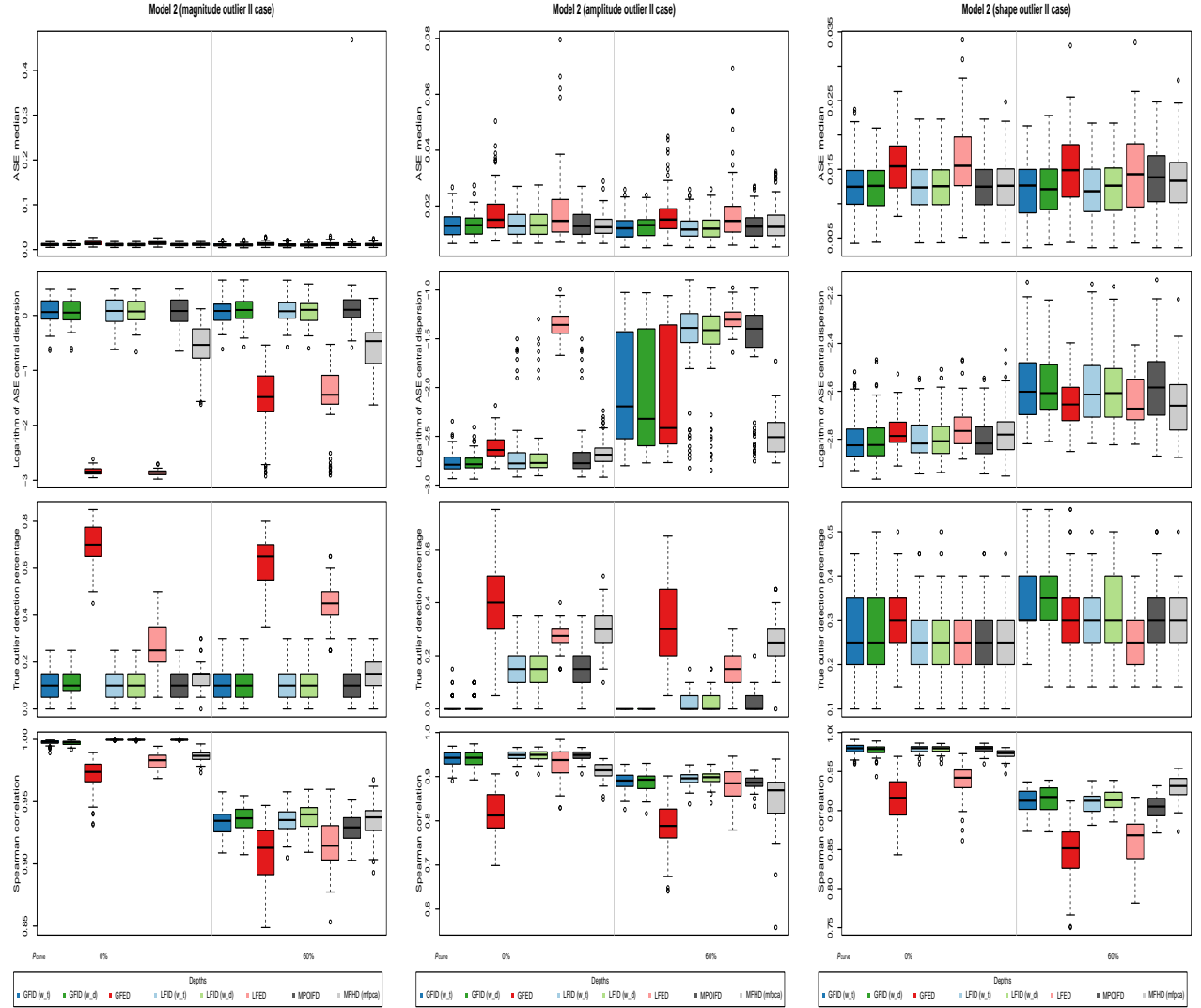


Figure S22: Left column shows Model 2 with magnitude outlier II, the middle column shows Model 2 with amplitude outlier II, and the right column shows Model 2 with shape outlier II. ASE of the estimated central curve (the first row), ASE of the 50%-dispersion curve (the second row), the outlier proportion in the lowest 10% depth region (the third row), and Spearman correlation (the fourth row). The sparseness type is **partial** sparseness with a dense case ($p_{curve} = 0\%$) and a high sparseness case ($p_{curve} \sim \mathcal{U}(0.4, 0.6)$).

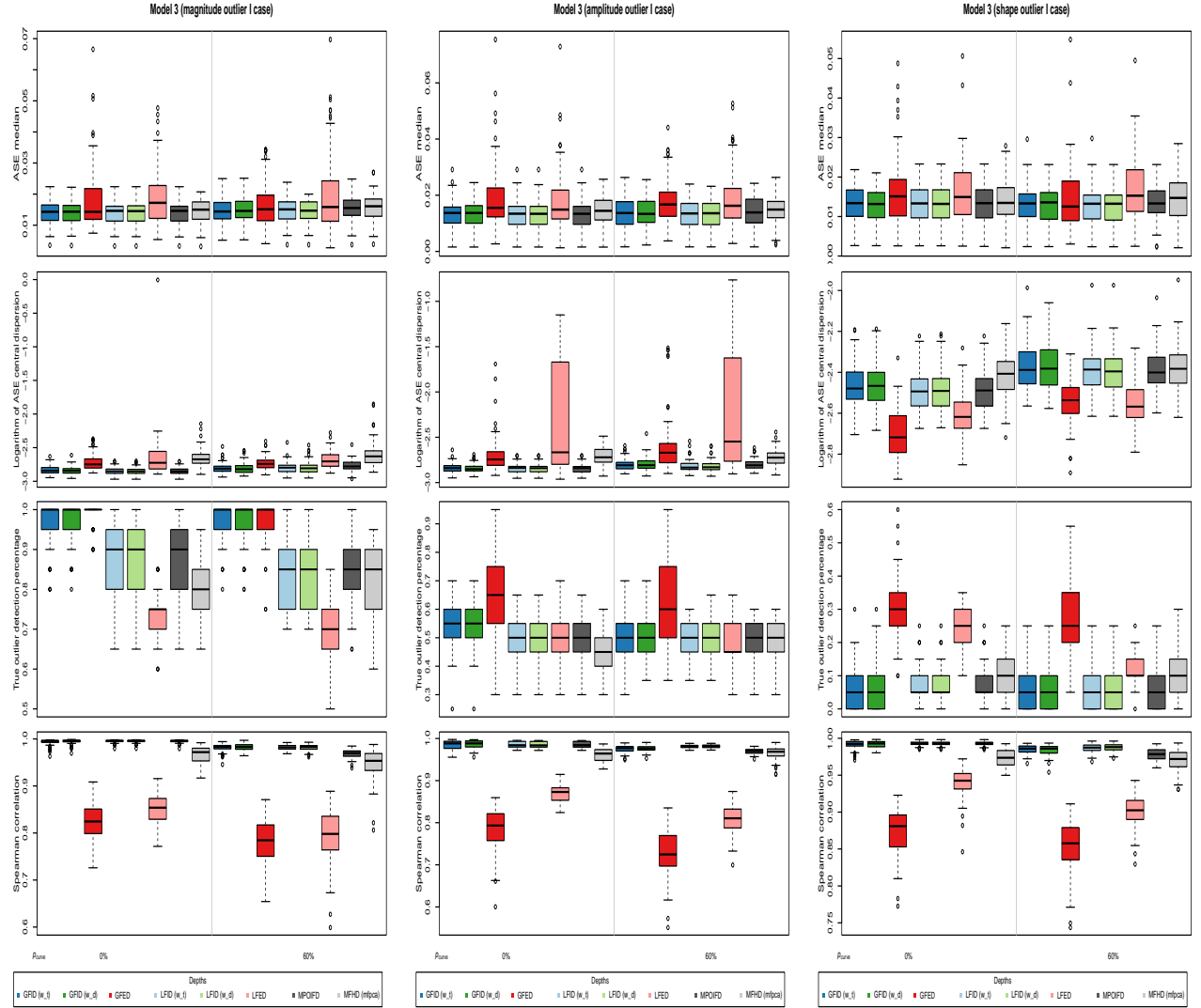


Figure S23: Left column shows Model 3 with magnitude outlier I, the middle column shows Model 3 with amplitude outlier I, and the right column shows Model 3 with shape outlier I. ASE of the estimated central curve (the first row), ASE of the 50%-dispersion curve (the second row), the outlier proportion in the lowest 10% depth region (the third row), and Spearman correlation (the fourth row). The sparseness type is **partial** sparseness with a dense case ($p_{curve} = 0\%$) and a high sparseness case ($p_{curve} \sim \mathcal{U}(0.4, 0.6)$).

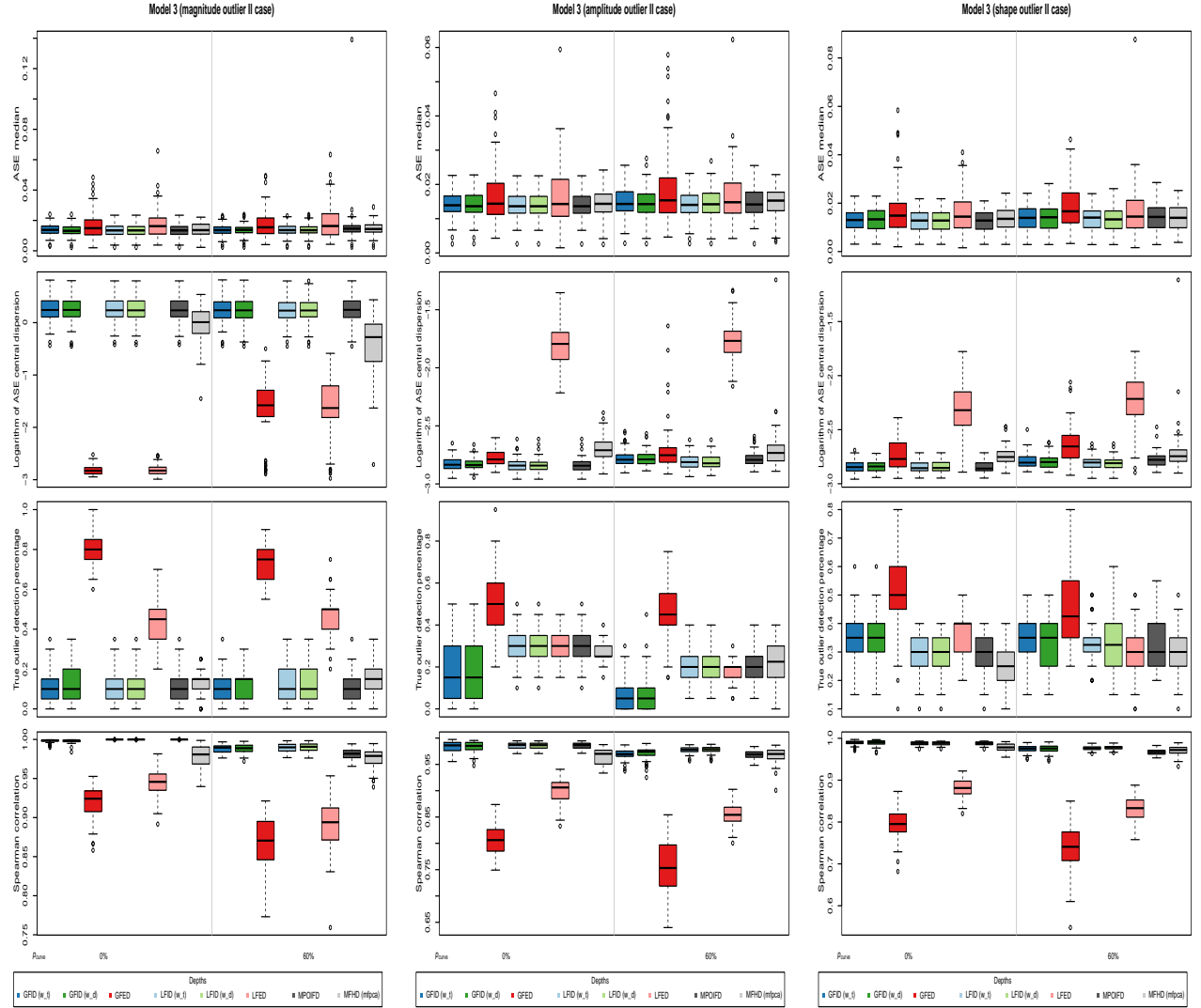


Figure S24: Left column shows Model 3 with magnitude outlier II, the middle column shows Model 3 with amplitude outlier II, and the right column shows Model 3 with shape outlier II. ASE of the estimated central curve (the first row), ASE of the 50%-dispersion curve (the second row), the outlier proportion in the lowest 10% depth region (the third row), and Spearman correlation (the fourth row). The sparseness type is **partial** sparseness with a dense case ($p_{curve} = 0\%$) and a high sparseness case ($p_{curve} \sim \mathcal{U}(0.4, 0.6)$).

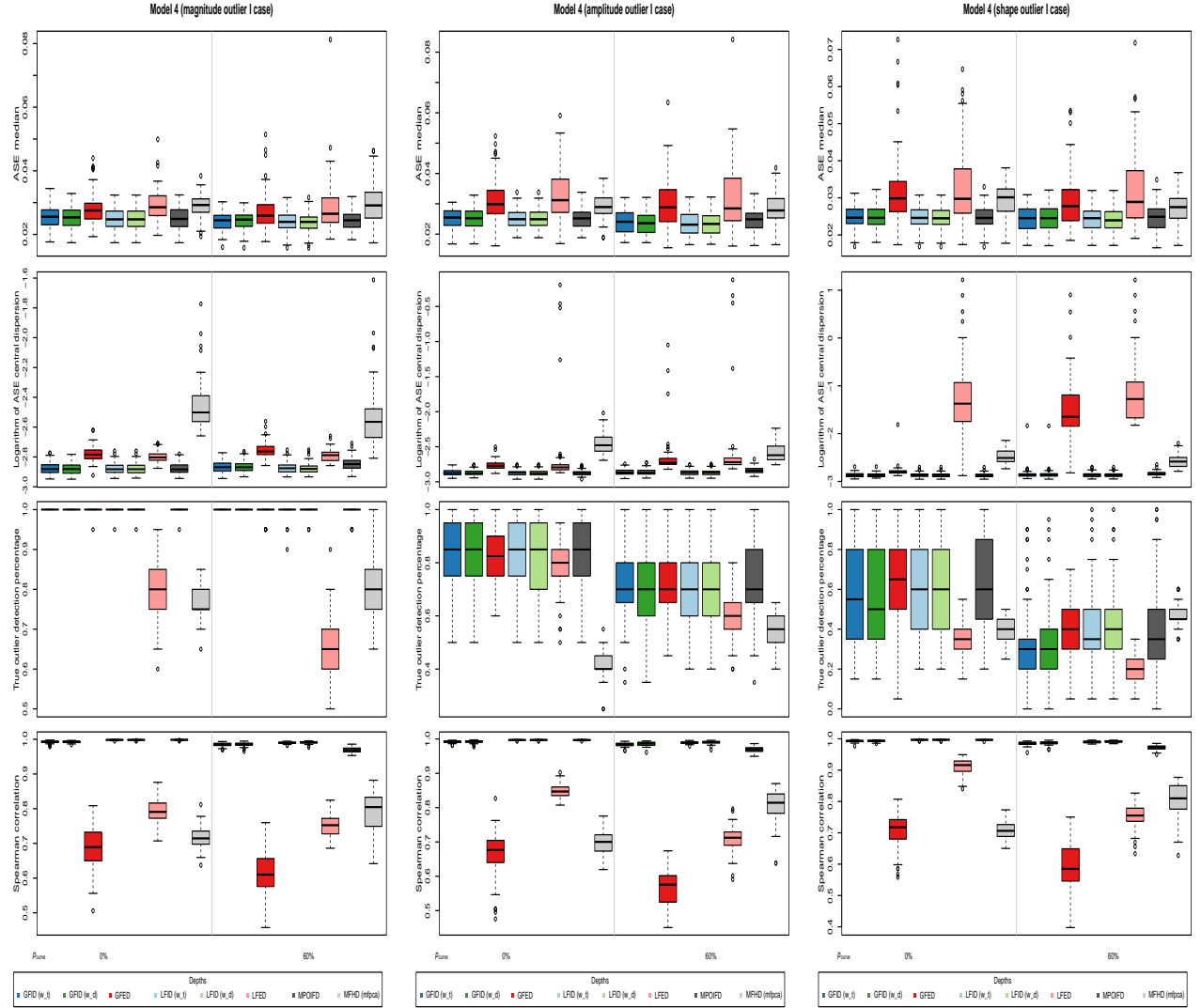


Figure S25: Left column shows Model 4 with magnitude outlier I, the middle column shows Model 4 with amplitude outlier I, and the right column shows Model 4 with shape outlier I. ASE of the estimated central curve (the first row), ASE of the 50%-dispersion curve (the second row), the outlier proportion in the lowest 10% depth region (the third row), and Spearman correlation (the fourth row). The sparseness type is **partial** sparseness with a dense case ($p_{curve} = 0\%$) and a high sparseness case ($p_{curve} \sim \mathcal{U}(0.4, 0.6)$).

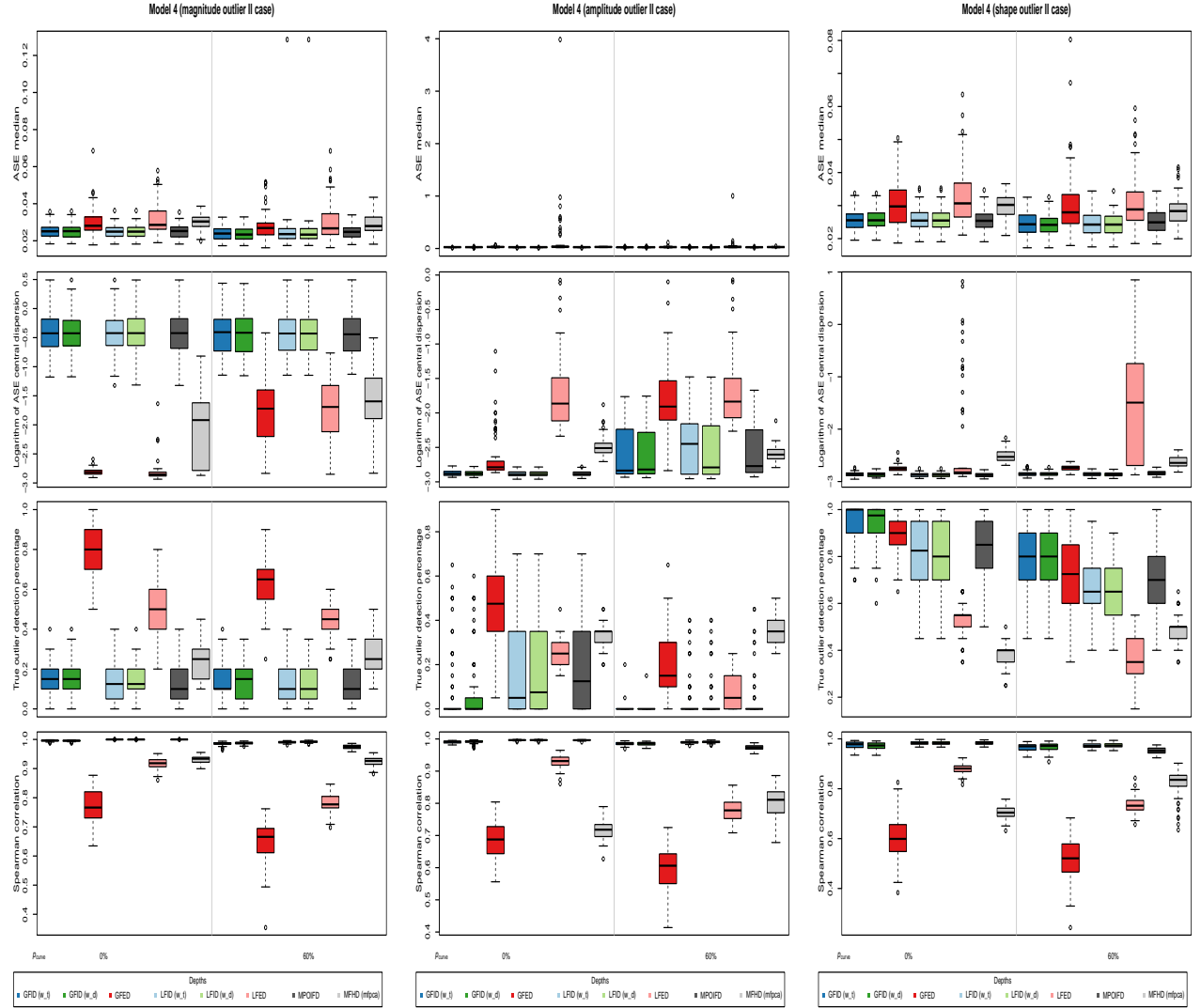


Figure S26: Left column shows Model 4 with magnitude outlier II, the middle column shows Model 4 with amplitude outlier II, and the right column shows Model 4 with shape outlier II. ASE of the estimated central curve (the first row), ASE of the 50%-dispersion curve (the second row), the outlier proportion in the lowest 10% depth region (the third row), and Spearman correlation (the fourth row). The sparseness type is **partial** sparseness with a dense case ($p_{curve} = 0\%$) and a high sparseness case ($p_{curve} \sim \mathcal{U}(0.4, 0.6)$).

2 Proofs

Before the proof, recall the definition of GMFD.

Definition 1 *Global Multivariate Functional Depth (GMFD, Population Version).*

Assume Conditions (A), (B.1) and (C), and the stochastic process $\mathbf{Y}^*(t)$ across time t is with cdf $F_{\mathbf{S}}$. From an arbitrary $\mathbf{X} \in \mathcal{C}^p(\mathcal{T})$, we obtain $\mathbf{X}^*(t) \in \mathbb{R}^p$ ($t \in \mathcal{T}$).

1. The **global multivariate functional integrated depth** (GMFID) is

$$GMFID(\mathbf{X}; F_{\mathbf{Y}}, \beta) = \int_{\mathcal{T}} D(\mathbf{X}^*(t); F_{\mathbf{S}}) \cdot w_{\beta}(t; F_{\mathbf{S}}) dt, \quad (1)$$

where $w_{\beta}(t; F_{\mathbf{S}})$ is the definition of $w_{\beta}(t; F_{\mathbf{Y}^*(t)})$ with the cdf $F_{\mathbf{S}}$ replacing $F_{\mathbf{Y}^*(t)}$.

2. The **global multivariate functional extremal depth** (GMFED) of \mathbf{X} is

$$MFED(\mathbf{X}; F_{\mathbf{Y}}) = 1 - P(\mathbf{X} \prec \mathbf{Y}) = P(\mathbf{X} \succeq \mathbf{Y}), \text{ where } \mathbf{Y} \sim F_{\mathbf{Y}}, \quad (2)$$

where $\Psi_{\mathbf{X}^*}(r) = \int_{\mathcal{T}} \mathbf{1}\{D(\mathbf{X}^*(t); F_{\mathbf{S}}) \leq r\} dt$.

Appendix

Proof of Theorem 1

1) We have $(\mathbf{A}\mathbf{X} + \widetilde{\mathbf{X}})^*(t) = (\mathbf{A}\Sigma_t \mathbf{A}^\top)^{-1/2} \{ \mathbf{A}\mathbf{X}(t) + \widetilde{\mathbf{X}}(t) - \mathbf{A}\mu_{\mathbf{X}}(t) - \widetilde{\mathbf{X}}(t) \} = (\mathbf{A}\Sigma_t \mathbf{A}^\top)^{-1/2} \mathbf{A} \{ \mathbf{X}(t) - \mu_{\mathbf{X}}(t) \} = (\mathbf{A}\Sigma_t \mathbf{A}^\top)^{-1/2} \mathbf{A}\Sigma_t^{1/2} \Sigma_t^{-1/2} \{ \mathbf{X}(t) - \mu_{\mathbf{X}}(t) \} = \mathbf{B}_t \mathbf{X}^*(t)$, where $\mathbf{B}_t = (\mathbf{A}\Sigma_t \mathbf{A}^\top)^{-1/2} \mathbf{A}\Sigma_t^{1/2}$.

Besides, $\mathbf{X}^*(t) \in \mathbb{R}^p$ for $t \in \mathcal{T}$ follow the same distribution as \mathbf{S} satisfying $E(\mathbf{S}) = \mathbf{0}$ and $\text{var}(\mathbf{S}) = \mathbf{I}_p$ with cdf $F_{\mathbf{S}}$.

We can obtain $E\{(\mathbf{A}\mathbf{X} + \widetilde{\mathbf{X}})^*(t)\} = \mathbf{0}$, $\text{var}\{(\mathbf{A}\mathbf{X} + \widetilde{\mathbf{X}})^*(t)\} = \mathbf{B}_t \text{var}\{\mathbf{X}^*(t)\} \mathbf{B}_t^\top = \mathbf{B}_t \mathbf{B}_t^\top = (\mathbf{A}\Sigma_t \mathbf{A}^\top)^{-1/2} \mathbf{A}\Sigma_t^{1/2} \Sigma_t^{1/2} \mathbf{A}^\top (\mathbf{A}\Sigma_t \mathbf{A}^\top)^{-1/2} = (\mathbf{A}\Sigma_t \mathbf{A}^\top)^{-1/2} \mathbf{A}\Sigma_t \mathbf{A}^\top (\mathbf{A}\Sigma_t \mathbf{A}^\top)^{-1/2} = \mathbf{I}_p$.

Hence, $(\mathbf{A}\mathbf{X} + \widetilde{\mathbf{X}})^*(t)$ also follow the distribution as \mathbf{S} . From the affine invariance of D , we have $D((\mathbf{A}\mathbf{X} + \widetilde{\mathbf{X}})^*(t); F_{(\mathbf{A}\mathbf{y} + \tilde{\mathbf{y}})^*(t)}) = D(\mathbf{X}^*(t); F_{\mathbf{Y}^*(t)})$. Then, $w_{\beta}(t; F_{(\mathbf{A}\mathbf{y} + \tilde{\mathbf{y}})^*}) = w(t; F_{\mathbf{Y}^*})$,

$$\Psi_{(\mathbf{A}\mathbf{X} + \widetilde{\mathbf{X}})^*}(d) = \Psi_{\mathbf{X}^*}(d) \text{ for } 0 \leq d \leq 1.$$

Therefore, $GMFD(\mathbf{X}; F_{\mathbf{Y}}, \beta) = GMFD(\mathbf{A}\mathbf{X} + \widetilde{\mathbf{X}}; F_{\mathbf{A}\mathbf{Y} + \widetilde{\mathbf{Y}}}, \beta)$.

2) For a center of symmetry $\Theta \in \mathcal{C}^p(\mathcal{T})$ such that $P_{\mathbf{Y}-\Theta} = P_{\Theta-\mathbf{Y}}$ for a stochastic process \mathbf{Y} , for each $t \in \mathcal{T}$, $\Theta(t)$ is a center of symmetry for $P_{\mathbf{Y}(t)}$. From definition 2.1 (ii) in [Zuo & Serfling \(2000a\)](#), $D(\Theta(t); F_{\mathbf{Y}(t)}) = \sup_{\mathbf{X}(t) \in \mathbb{R}^p} D(\mathbf{X}(t); F_{\mathbf{Y}(t)})$ for $t \in \mathcal{T}$. From the affine invariance of D , we have $D(\Theta^*(t); F_{\mathbf{Y}^*(t)}) = \sup_{\mathbf{X}^*(t) \in \mathbb{R}^p} D(\mathbf{X}^*(t); F_{\mathbf{Y}^*(t)})$ with $\mathbf{X}^*(t) = \Sigma_t^{-1/2}\{\mathbf{X}(t) - \boldsymbol{\mu}(t)\}$, and $\Theta^*(t) = \Sigma_t^{-1/2}\{\Theta(t) - \boldsymbol{\mu}(t)\}$. Hence, $\Theta^*(t)$ is a center of symmetry for $P_{\mathbf{Y}^*(t)}$.

According to the definition of GMFID in Equation (1), since D has maximality at the center $\Theta(t)$, GMFID has maximality at Θ .

According to the definition of GMFED in Equation (1), for any $0 < r < 1$, there exists $\mathcal{U}_r \subset \mathcal{T}$, $\forall t \in \mathcal{U}_r$, $D(\Theta^*(t), F_{\mathbf{Y}^*(t)}) \leq r$; and $\forall t \in \mathcal{T} \setminus \mathcal{U}_r$, $D(\Theta^*(t), F_{\mathbf{Y}^*(t)}) > r$. That is, $\Psi_{\Theta^*}(r) = \frac{|\mathcal{U}_r|}{|\mathcal{T}|}$. If there exists \mathbf{X}^* such that $\mathbf{X}^* \succ \Theta^*$, then we have $0 < r_0 < 1$ such that when $0 < r < r_0$, we have $\Psi_{\mathbf{X}^*}(r) = \Psi_{\Theta^*}(r)$, and $\Psi_{\mathbf{X}^*}(r_0) < \Psi_{\Theta^*}(r_0)$. There exists $\mathcal{U}_{r_0} \subset \mathcal{T}$, for $t \in \mathcal{U}_{r_0}$ such that $D(\Theta^*(t), F_{\mathbf{Y}^*(t)}) \leq r_0$, and when $t \in \mathcal{T} \setminus \mathcal{U}_{r_0}$, we have $D(\Theta^*(t), F_{\mathbf{Y}^*(t)}) > r_0$. Hence, $\Psi_{\Theta^*}(r_0) = \frac{|\mathcal{U}_{r_0}|}{|\mathcal{T}|}$.

When $t \in \mathcal{U}_{r_0}$, we have $D(\mathbf{X}^*(t); F_{\mathbf{Y}^*(t)}) \leq D(\Theta^*(t), F_{\mathbf{Y}^*(t)}) \leq r_0$. Then, $\Psi_{\mathbf{X}^*}(r_0) \geq \Psi_{\Theta^*}(r_0)$ is in conflict with $\Psi_{\mathbf{X}^*}(r_0) < \Psi_{\Theta^*}(r_0)$ when $\mathbf{X}^* \succ \Theta^*$. According to the ranking criteria, $\forall \mathbf{X}^* \in \mathbb{R}^p$, $\mathbf{X}^* \preceq \Theta^*$, and Θ^* is the one with highest depth 1 in GMFED.

3) From the proof of (2) in Theorem 1 that $\Theta^*(t)$ is the center of $F_{\mathbf{Y}^*(t)}$ and the monotonicity relative to the deepest partial of D , we have $D(\mathbf{X}^*(t); F_{\mathbf{Y}^*(t)}) \leq D(\Theta^*(t) + a\{\mathbf{X}^*(t) - \Theta^*(t)\}; F_{\mathbf{Y}^*(t)})$ for $a \in [0, 1]$.

From the definition of Equation (1), the weight $w_\beta(t; F_{\mathbf{Y}^*(t)})$ does not change, and hence, $GMFID(\mathbf{X}; F_{\mathbf{Y}}, \beta) \leq GMFID(\Theta + a(\mathbf{X} - \Theta); F_{\mathbf{Y}}, \beta)$.

For any $0 < r < 1$, there exists $\mathcal{U}_r \subset \mathcal{T}$ such that $\Psi_{\Theta^* + a(\mathbf{X}^* - \Theta^*)}(r) = \frac{|\mathcal{U}_r|}{|\mathcal{T}|}$; that is, $\forall t \in \mathcal{U}_r$, $D(\Theta^*(t) + a\{\mathbf{X}^*(t) - \Theta^*(t)\}; F_{\mathbf{Y}^*(t)}) \leq r$; $\forall t \in \mathcal{T} \setminus \mathcal{U}_r$, $D(\Theta^*(t) + a\{\mathbf{X}^*(t) - \Theta^*(t)\}; F_{\mathbf{Y}^*(t)}) > r$. If there exists \mathbf{X} such that $GMFED(\mathbf{X}; F_{\mathbf{Y}}) > GMFED(\Theta + a(\mathbf{X} - \Theta); F_{\mathbf{Y}})$, then there exists

\mathbf{X}^* such that $\mathbf{X}^* \succ \Theta^* + a(\mathbf{X}^* - \Theta^*)$, and then, we have an $0 < r_0 < 1$ such that when $0 < r < r_0$, we have $\Psi_{\mathbf{X}^*}(r) = \Psi_{\Theta^*}(r)$, and $\Psi_{\mathbf{X}^*}(r_0) < \Psi_{\Theta^*+a(\mathbf{X}^*-\Theta^*)}(r_0)$. There exists $\mathcal{U}_{r_0} \subset \mathcal{T}$ for $t \in \mathcal{U}_{r_0}$ such that $D(\Theta^*(t) + a(\mathbf{X}^*(t) - \Theta^*(t)), F_{\mathbf{Y}^*(t)}) \leq r_0$, and when $t \in \mathcal{T} \setminus \mathcal{U}_{r_0}$, we have $D(\Theta^*(t) + a(\mathbf{X}^* - \Theta^*), F_{\mathbf{Y}^*(t)}) > r_0$. Hence, $\Psi_{\Theta^*}(r_0) = \frac{|\mathcal{U}_{r_0}|}{|\mathcal{T}|}$.

When $t \in \mathcal{U}_{r_0}$, we have $D(\mathbf{X}^*(t); F_{\mathbf{Y}^*(t)}) \leq D(\Theta^*(t) + a\{\mathbf{X}^*(t) - \Theta^*(t)\}; F_{\mathbf{Y}^*(t)}) \leq r_0$. Thus, $\Psi_{\mathbf{X}^*}(r_0) \geq \Psi_{\Theta^*+a(\mathbf{X}^*-\Theta^*)}(r_0)$. Hence, $\mathbf{X}^* \preceq \Theta^* + a(\mathbf{X}^* - \Theta^*)$ and conflicts with $\mathbf{X}^* \succ \Theta^* + a(\mathbf{X}^* - \Theta^*)$. Hence, $GMFED(\mathbf{X}; F_{\mathbf{Y}}) \leq GMFED(\Theta + a(\mathbf{X} - \Theta); F_{\mathbf{Y}})$.

4) From the vanishing at infinity of D , for $t \in \mathcal{T}$ and $\mathbf{X}_n(t) \in \mathbb{R}^p$, if $\|\mathbf{X}_n(t)\| \rightarrow \infty$, then $\lim_{n \rightarrow \infty} D(\mathbf{X}_n(t); F_{\mathbf{Y}(t)}) = 0$. From the affine invariance of D , $\lim_{n \rightarrow \infty} D(\mathbf{X}_n(t); F_{\mathbf{Y}(t)}) = \lim_{n \rightarrow \infty} D(\mathbf{X}_n^*(t); F_{\mathbf{Y}^*(t)}) = 0$.

Since we have $\lim_{n \rightarrow \infty} D(\mathbf{X}_n^*(t); F_{\mathbf{Y}^*(t)}) = 0$ for almost all time points $t \in \mathcal{T}$, according to Equation (1), $\lim_{n \rightarrow \infty} GMFID(\mathbf{X}_n; F_{\mathbf{Y}}, \beta) = 0$.

Next, $\forall C > 0$, $\exists n' > 0$, when $n > n'$ such that $D(\mathbf{X}_n^*(t), F_{\mathbf{Y}^*(t)}) \leq C$ for almost all points $t \in \mathcal{T}$. Let $C = \frac{1}{n}$. From the right continuity of Ψ , $\lim_{\frac{1}{n} \rightarrow 0^+} \Psi_{\mathbf{X}_n^*}(1/n) = \Psi_{\mathbf{X}^*}(0) = 1$; hence, \mathbf{X}_n^* is the most extremal curve when $n \rightarrow \infty$. According to Equation (1), $\lim_{n \rightarrow \infty} GMFED(\mathbf{X}_n; F_{\mathbf{Y}_n}) = \lim_{n \rightarrow \infty} 1/n = 0$.

Proof of Theorem 2

1) We use Berge's maximum theorem (e.g., [Abalo & Kostreva 2005](#), Theorem 1). Consider the function $D : \mathcal{T} \times \mathbb{R}^p \rightarrow \mathbb{R} : (t, \mathbf{x}) \mapsto D(\mathbf{x}, F_{\mathbf{Y}(t)})$. The continuity of Θ follows from the continuity of $\mathbf{x}(t)$ and D .

2) For any $t \in \mathcal{T}$, there exists a point $\Theta(t) \in \mathbb{R}^p$ with the maximum depth for $F_{\mathbf{Y}(t)}$ such that $D(\Theta(t), F_{\mathbf{Y}(t)}) = \max_{\mathbf{X}(t) \in \mathbb{R}^p} D(\mathbf{X}(t), F_{\mathbf{Y}(t)})$. From the affine invariance of D , the deepest point Θ in \mathbf{Y} ensures the deepest point Θ^* in \mathbf{Y}^* . From Definition 1, we have $GMFID(\mathbf{X}; F_{\mathbf{Y}}, \beta) \leq GMFID(\Theta; F_{\mathbf{Y}}, \beta)$ for $\mathbf{X} \in \mathcal{C}^p(\mathcal{T})$.

Similar to the proof in 2) in Theorem 1, if there exists Θ with the maximum depth at every time point, then $GMFED(\Theta; F_{\mathbf{Y}}) \leq GMFED(\mathbf{X}; F_{\mathbf{Y}})$ for $\mathbf{X} \in \mathcal{C}^p(\mathcal{T})$.

3) We prove by contradiction that a deepest curve implies the existence of deepest points at every $t \in \mathcal{T}$. We denote the deepest point of $P_{\mathbf{Y}}$ by $\tilde{\boldsymbol{\theta}}_t = \tilde{\Theta}(t)$. Suppose that there exists a $t_1 \in \mathcal{T}$ with $D(\Theta(t_1); F_{\mathbf{Y}(t_1)}) < D(\tilde{\boldsymbol{\theta}}_{t_1}; F_{\mathbf{Y}(t_1)})$. According to Lemma 2 in [Claeskens et al. \(2014\)](#), there exists a $\delta_0 > 0$ with for $|tt_1| < \delta : D(\Theta(t); F_{\mathbf{Y}(t)}) < D(\tilde{\boldsymbol{\theta}}_{t_1}; F_{\mathbf{Y}(t)}) < D(\tilde{\boldsymbol{\theta}}_t; F_{\mathbf{Y}(t)}) \leq \tilde{r}$.

$$\begin{aligned} \text{For GMFID, we have } & GMFID(\Theta; F_{\mathbf{Y}}, \beta) = \int_{\mathcal{T}} D(\Theta^*(t); F_{\mathbf{S}}) w_{\beta}(t; F_{\mathbf{S}}) dt \\ & < \int_{|t-t_1|>\delta_0} D(\Theta^*(t); F_{\mathbf{S}}) w_{\beta}(t; F_{\mathbf{S}}) dt + \int_{t_1-\delta_0}^{t_1+\delta_0} D(\tilde{\boldsymbol{\theta}}(t); F_{\mathbf{S}}) w_{\beta}(t; F_{\mathbf{S}}) dt \\ & \leq GMFID(\tilde{\Theta}; F_{\mathbf{Y}}, \beta), \text{ which is in contradiction with the fact that } \Theta \text{ is a deepest curve.} \end{aligned}$$

For GMFED, we can easily get $\Psi_{\tilde{\Theta}}(r) = \Psi_{\Theta}(r)$ for $0 \leq r \leq \inf_{|t-t_1|<\delta_0} D(\Theta(t); F_{\mathbf{Y}(t)})$, and $\Psi_{\Theta}(r) > \Psi_{\tilde{\Theta}}(r)$ for $r > \inf_{|t-t_1|<\delta_0} D(\Theta(t); F_{\mathbf{Y}(t)})$. Hence, $\Theta \prec \tilde{\Theta}$, which is in conflict with the fact that Θ is the deepest curve.

Finite sample GMFID Calculation of Definition 3

To apply Definition 1 to the curve observations in a grid of time points, we use the linear interpolation at the unobserved time points and the middle time points between $\mathcal{T}_j^N = [t_{j-1}^N, t_j^N]$ ($j = 1, \dots, \bar{T}$) with the average of the function values. This yields a sample of continuous p -variate stochastic processes $\tilde{\mathbf{Y}}_i$ and $\tilde{\mathbf{Y}}_i^*$, ($i = 1, \dots, N$) on the interval $\mathcal{T}^N = [t_1^N, t_{\bar{T}}^N]$ in which the l th ($l = 1, \dots, p$) component is defined by

$$\begin{aligned} \tilde{Y}_i^{(l)}(t) &= \begin{cases} Y_i^{(l)}(t_j^N) \frac{t_j^N + t_{j+1}^N - 2t}{t_{j+1}^N - t_j^N} \mathbf{1}_{t_j^N}(t) + \overline{Y^{(l)}}(t_j^N) \{1 - \frac{t_j^N + t_{j+1}^N - 2t}{t_{j+1}^N - t_j^N} \mathbf{1}_{t_j^N}(t)\} & t \in [t_j^N, (t_j^N + t_{j+1}^N)/2], \\ Y_i^{(l)}(t_{j+1}^N) \frac{2t - t_j^N - t_{j+1}^N}{t_{j+1}^N - t_j^N} \mathbf{1}_{t_{j+1}^N}(t) + \overline{Y^{(l)}}(t_j^N) \{1 - \frac{2t - t_j^N - t_{j+1}^N}{t_{j+1}^N - t_j^N} \mathbf{1}_{t_{j+1}^N}(t)\} & t \in [(t_j^N + t_{j+1}^N)/2, t_{j+1}^N], \end{cases} \\ \text{where } \mathbf{1}_A(x) &:= \begin{cases} 1 & \text{if } x \in A, \\ 0 & \text{if } x \notin A, \end{cases} \text{ and } \overline{Y^{(l)}}(t_j^N) = \frac{\sum_{i=1}^N Y_i^{(l)}(t_j^N) \mathbf{1}_{t_j^N}(t)}{\sum_{i=1}^N \mathbf{1}_{t_j^N}(t)} \text{ for } j = 1, \dots, \bar{T}. \end{aligned}$$

The empirical cumulative distribution function of this sample is denoted by $F_{\tilde{\mathbf{Y}},N}$. Then

$$\tilde{Y}_i^{(l)*}(t) = \begin{cases} \widehat{Y}_i^{(l)*}(t_j^N) \frac{t_j^N + t_{j+1}^N - 2t}{t_{j+1}^N - t_j^N} \mathbf{1}_{t_j^N}(t) + \widehat{\overline{Y}^{(l)*}}(t_j^N) \{1 - \frac{t_j^N + t_{j+1}^N - 2t}{t_{j+1}^N - t_j^N} \mathbf{1}_{t_j^N}(t)\} & t \in [t_j^N, (t_j^N + t_{j+1}^N)/2], \\ \widehat{Y}_i^{(l)*}(t_{j+1}^N) \frac{2t - t_j^N - t_{j+1}^N}{t_{j+1}^N - t_j^N} \mathbf{1}_{t_{j+1}^N}(t) + \widehat{\overline{Y}^{(l)*}}(t_j^N) \{1 - \frac{2t - t_j^N - t_{j+1}^N}{t_{j+1}^N - t_j^N} \mathbf{1}_{t_{j+1}^N}(t)\} & t \in [(t_j^N + t_{j+1}^N)/2, t_{j+1}^N], \end{cases}$$

where $\widehat{\mathbf{Y}}^*(t_j^N) = (\widehat{Y}^{(1)*}(t_j^N), \dots, \widehat{Y}^{(p)*}(t_j^N))^{\top}$, $\overline{Y^{(l)}}(t_j^N) \approx \frac{\sum_{g=1}^N \sum_{h=1}^{T_g} Y_g^{(l)}(t_{g,h}) \mathbf{1}_{(t_{g,h} \in \mathcal{T}_j^N)}}{\sum_{g=1}^N \sum_{h=1}^{T_g} \mathbf{1}_{(t_{g,h} \in \mathcal{T}_j^N)}}$ for $j = 1, \dots, \bar{T} - 1$. The empirical cumulative distribution function of this sample is denoted by $F_{\tilde{\mathbf{Y}}^*,N}$.

Note the definition of the p -variate processes $\tilde{\mathbf{Y}}_i$ and the affine invariance of the depth function $D(\tilde{\mathbf{X}}^*(t_j^N); F_{\tilde{\mathbf{Y}}^*(t_j^N), N}) = D(\widehat{\mathbf{X}}^*(t_j^N); F_{\widehat{\mathbf{Y}}^*(t_j^N), N})$. In addition, for $\mathbf{X} \in \mathcal{C}^p(\mathcal{T})$ from the stochastic process \mathbf{Y} with cdf $F_{\mathbf{Y}}$, and $\mathbf{A} \in \mathbb{R}^{p \times p}$ with $\det(\mathbf{A}) \neq 0$ and $\widetilde{\mathbf{X}} \in \mathcal{C}^p(\mathcal{T})$, $\mathbf{A}\mathbf{X} + \tilde{\mathbf{X}}$ on $\mathcal{C}^p(\mathcal{T})$ has cdf $F_{\mathbf{A}\mathbf{Y} + \tilde{\mathbf{Y}}}$.

We consider two scenarios: 1) w is proportional to the volume of the depth range, and 2) w is proportional to the time density.

1) For $t \in \mathcal{T}$, $\text{vol}\{D_\beta(t, \mathbf{Y}(t))\} = |\det(\mathbf{A})| \cdot \text{vol}\{D_\beta(t, \mathbf{A}\mathbf{Y}(t) + \tilde{\mathbf{Y}}(t))\}$.

For $t \in [t_j^N, (t_j^N + t_{j+1}^N)/2]$, $\mathbf{A}_{N_j}(t) = \frac{t_j^N + t_{j+1}^N - 2t}{t_{j+1}^N - t_j^N} \mathbf{I}_p$; for $t \in [(t_j^N + t_{j+1}^N)/2, t_{j+1}^N]$, $\det\{\mathbf{A}_{N_j}(t)\} = -\frac{t_j^N + t_{j+1}^N - 2t}{t_{j+1}^N - t_j^N} \mathbf{I}_p$. Hence, for $t \in [t_j^N, t_{j+1}^N]$, $|\det\{\mathbf{A}_{N_j}(t)\}| = |\frac{t_j^N + t_{j+1}^N - 2t}{t_{j+1}^N - t_j^N}|^p$.

Indeed, when $w \propto$ the volume of the depth range,

$$\begin{aligned} GMFID(\mathbf{X}; F_{\tilde{\mathbf{Y}}_N}, \beta) &= \sum_{j=1}^{\bar{T}-1} \int_{t_j^N}^{t_{j+1}^N} D(\widehat{\mathbf{X}}^*(t_j^N); F_{\widehat{\mathbf{Y}}^*(t_j^N), N}) w_\beta(t; F_{\tilde{\mathbf{Y}}^*(t), N}) dt \\ &= \sum_{j=1}^{\bar{T}-1} \left\{ D(\widehat{\mathbf{X}}^*(t_j^N); F_{\widehat{\mathbf{Y}}^*(t_j^N), N}) \frac{\text{vol}\{D_\beta(t_j^N, F_{\widehat{\mathbf{Y}}^*(t_j^N), N})\}}{\int_{\mathcal{T}^N} \text{vol}\{D_\beta(u, F_{\widehat{\mathbf{Y}}^*(u), N})\} du} \int_{t_j^N}^{(t_j^N + t_{j+1}^N)/2} |\det\{\mathbf{A}_{N_j}(t)\}| dt + \right. \\ &\quad \left. D(\widehat{\mathbf{X}}^*(t_{j+1}^N); F_{\widehat{\mathbf{Y}}^*(t_{j+1}^N), N}) \frac{\text{vol}\{D_\beta(t_{j+1}^N, F_{\widehat{\mathbf{Y}}^*(t_{j+1}^N), N})\}}{\int_{\mathcal{T}^N} \text{vol}\{D_\beta(u, F_{\widehat{\mathbf{Y}}^*(u), N})\} du} \int_{(t_j^N + t_{j+1}^N)/2}^{t_{j+1}^N} |\det\{\mathbf{A}_{N_j}(t)\}| dt \right\}. \\ \text{Knowing } \int_{t_j^N}^{(t_j^N + t_{j+1}^N)/2} |\det\{\mathbf{A}_{N_j}(t)\}| dt &= \int_{(t_j^N + t_{j+1}^N)/2}^{t_{j+1}^N} |\det\{\mathbf{A}_{N_j}(t)\}| dt = \frac{t_{j+1}^N - t_j^N}{2(p+1)}, \text{ and} \\ \int_{\mathcal{T}^N} \text{vol}\{D_\beta(u, F_{\widehat{\mathbf{Y}}^*(u), N})\} du &= \sum_{j=1}^{\bar{T}-1} \left\{ \text{vol}\{D_\beta(t_j^N, F_{\widehat{\mathbf{Y}}^*(t_j^N), N})\} \frac{t_{j+1}^N - t_j^N}{2(p+1)} + \right. \\ &\quad \left. \text{vol}\{D_\beta(t_{j+1}^N, F_{\widehat{\mathbf{Y}}^*(t_{j+1}^N), N})\} \frac{t_{j+1}^N - t_{j-1}^N}{2(p+1)} \right\} = \sum_{j=1}^{\bar{T}} \text{vol}\{D_\beta(t_j^N, F_{\widehat{\mathbf{Y}}^*(t_j^N), N})\} \frac{t_{j+1}^N - t_{j-1}^N}{2(p+1)}. \end{aligned}$$

Hence, GMFID when w is proportional to the volume of the depth range is transformed to

$$GMFID(\mathbf{X}; F_{\tilde{\mathbf{Y}}_N}, \beta) = \sum_{j=1}^T D(\widehat{\mathbf{X}}^*(t_j^N); F_{\widehat{\mathbf{Y}}^*(t_j^N), N}) \frac{\text{vol}\{D_\beta(t_j^N, F_{\widehat{\mathbf{Y}}^*(t_j^N), N})\} (t_{j+1}^N - t_{j-1}^N)}{\sum_{j=1}^{\bar{T}} \text{vol}\{D_\beta(t_j^N, F_{\widehat{\mathbf{Y}}^*(t_j^N), N})\} (t_{j+1}^N - t_{j-1}^N)}.$$

2) Let $g_{N,k}(t) = \sum_{e=1}^N \sum_{h=1}^{T_e} \mathbf{1}(t_{e,h} \in \mathcal{T}_k^N)$.

$$\begin{aligned} GMFID(\mathbf{X}; F_{\tilde{\mathbf{Y}}_N}, \beta) &= \sum_{j=1}^{\bar{T}-1} \int_{t_j^N}^{t_{j+1}^N} D(\widehat{\mathbf{X}}^*(t_j^N); F_{\widehat{\mathbf{Y}}^*(t_j^N), N}) w_\beta(t; F_{\tilde{\mathbf{Y}}^*(t), N}) dt \\ &= \sum_{j=1}^{\bar{T}-1} \int_{t_j^N}^{t_{j+1}^N} D(\widehat{\mathbf{X}}^*(t_j^N); F_{\widehat{\mathbf{Y}}^*(t_j^N), N}) \frac{g_{N,j}(t)}{\sum_{j=1}^{\bar{T}-1} \int_{t_j^N}^{t_{j+1}^N} g_{N,j}(t) dt} dt \\ &= \sum_{j=1}^{\bar{T}-1} D(\widehat{\mathbf{X}}^*(t_j^N); F_{\widehat{\mathbf{Y}}^*(t_j^N), N}) \frac{g_{N,j}(t_j^N) (t_{j+1}^N - t_j^N)}{\sum_{j=1}^{\bar{T}} g_{N,j}(t_j^N) (t_{j+1}^N - t_j^N)}. \end{aligned}$$

Proof of Lemma 1

1) From the strong law of large numbers, the pointwise sample mean function $\bar{\mathbf{Y}}(t_{i,k})$ converges

almost surely towards the pointwise mean $E\{\mathbf{Y}(t_{i,k})\}$, and the pointwise sample covariance $\mathbf{Q}_{t_{i,k}}$ converges in probability towards the variance $\Sigma_{t_{i,k}}$, i.e., $\bar{\mathbf{Y}}(t_{i,k}) \xrightarrow{a.s.} E\{\mathbf{Y}(t_{i,k})\}$, and $\mathbf{Q}_{t_{i,k}} \xrightarrow{a.s.} \Sigma_{t_{i,k}}$.

When $T_s \rightarrow \infty$, $\lim_{T_s \rightarrow \infty} \bar{Y}^{(l)}(t_{i,k}) = \frac{\lim_{T_s \rightarrow \infty} \sum_{g=1}^N \sum_{h=1}^{T_g} Y_g^{(l)} \mathbf{1}(t_{g,h} \in \mathcal{T}_j^N)}{\lim_{T_s \rightarrow \infty} \sum_{g=1}^N \sum_{h=1}^{T_g} \mathbf{1}(t_{g,h} \in \mathcal{T}_j^N)} = \frac{\sum_{g=1}^N Y_g^{(l)}(t_{i,k}) m_g}{\sum_{g=1}^N m_g} = \frac{1}{M_N} \sum_{g=1}^N m_g Y_g^{(l)}(t_{i,k})$ with $m_g = \sum_{h=1}^{T_g} \mathbf{1}(t_{g,h} \in \mathcal{T}_j^N)$, $M_N = \sum_{g=1}^N m_g$, and $0 \leq m_g \leq T_g$.

Let $M_N \rightarrow \infty$ when $N \rightarrow \infty$. If $\sup_{N \geq 1} \frac{N m_N}{M_N} < \infty$, and $\sup_{N \geq 2} \sum_{i=1}^{N-1} \frac{i|m_{i+1}-m_i|}{M_N} < \infty$, and $\frac{1}{N} \sum_{g=1}^N Y_g^{(l)}(t_{i,k}) \xrightarrow{a.s.} E\{\mathbf{Y}^{(l)}(t_{i,k})\}$, then according to Theorem 1 (Etemadi 2006), we have $\bar{Y}^{(l)}(t_{i,k}) \xrightarrow{a.s.} E\{\mathbf{Y}^{(l)}(t_{i,k})\}$ as $T_s \rightarrow \infty$ and $N \rightarrow \infty$.

2) Similarly, we can prove $\bar{Y}^{(l)} \bar{Y}^{(m)}(t_{i,k}) \xrightarrow{a.s.} E\{\mathbf{Y}^{(l)}(t_{i,k}) \mathbf{Y}^{(m)}(t_{i,k})\}$. Hence, for any $1 \leq l, m \leq p$, we have $\bar{Y}^{(l)} \bar{Y}^{(m)}(t_{i,k}) - \bar{Y}^{(l)}(t_{i,k}) \bar{Y}^{(m)}(t_{i,k}) \xrightarrow{a.s.} \text{cov}\{Y^{(l)}(t_{i,k}), Y^{(m)}(t_{i,k})\}$ as $T_s \rightarrow \infty$ and $N \rightarrow \infty$.

Proof of Theorem 3

1) From Definition 1,

$$\begin{aligned} \sup_{\mathbf{X} \in \mathcal{C}^p(\mathcal{T})} |GMFID_N(\mathbf{X}; F_{\mathbf{Y}_N}, \beta) - GMFID(\mathbf{X}; F_{\mathbf{Y}}, \beta)| &\leq \sup_{\mathbf{X} \in \mathcal{C}^p(\mathcal{T})} \left\{ \int_{t \in \mathcal{T}} |D(\widehat{\mathbf{X}}^*(t); F_{\tilde{\mathbf{Y}}^*(t), N}) - D(\mathbf{X}^*(t); F_{\mathbf{Y}^*(t)})| dt \right. \\ &\quad \left. + \int_{t \in \mathcal{T}} |w_\beta(t; F_{\tilde{\mathbf{Y}}^*(t), N}) - w_\beta(t; F_{\mathbf{Y}^*(t), N})| dt \right\} \leq \sup_{\mathbf{X} \in \mathcal{C}^p(\mathcal{T})} \left\{ \int_{t \in \mathcal{T}} |D(\widehat{\mathbf{X}}^*(t); F_{\tilde{\mathbf{Y}}^*(t), N}) - D(\mathbf{X}^*(t); F_{\tilde{\mathbf{Y}}^*(t), N})| dt \right. \\ &\quad \left. + \int_{t \in \mathcal{T}} |D(\mathbf{X}^*(t); F_{\tilde{\mathbf{Y}}^*(t), N}) - D(\mathbf{X}^*(t); F_{\mathbf{Y}^*(t)})| dt + \int_{t \in \mathcal{T}} |w_\beta(t; F_{\tilde{\mathbf{Y}}^*(t), N}) - w_\beta(t; F_{\mathbf{Y}^*(t)})| dt \right\}. \end{aligned}$$

Then the proof is separated into three parts.

(i). From the strong law of large numbers, we have $\bar{\mathbf{Y}}(t_{i,k}) \xrightarrow{a.s.} E\{\mathbf{Y}(t_{i,k})\}$, and $\mathbf{Q}_{t_{i,k}} \xrightarrow{a.s.} \Sigma_{t_{i,k}}$.

The inverse and the power of a symmetric and positive definite matrix is continuous. From the continuous mapping theorem, $\widehat{\mathbf{Y}}_N^*(t_{i,k}) \xrightarrow{a.s.} \mathbf{Y}^*(t_{i,k})$.

(ii). In the space of curves in $\mathcal{C}^p(\mathcal{T})$, we define the uniform distance $\rho(\mathbf{X}, \mathbf{Y}) = \|\mathbf{X} - \mathbf{Y}\|_\infty = \sup_{t \in \mathcal{T}} \|\mathbf{X}(t) - \mathbf{Y}(t)\|$, with $\|\cdot\|$ the Euclidean norm in \mathbb{R}^p . We first show that the function $\{\tilde{\mathbf{Y}}_i^* = (\tilde{\mathbf{Y}}_i^{*(1)}, \dots, \tilde{\mathbf{Y}}_i^{*(p)})^\top \in \mathbb{R}^p, i = 1, \dots, N, t \in \mathcal{T}^N\} \xrightarrow{P} \mathbf{Y}^*$. From Conditions (B.1)–(B.2), we have $|G(t_{i,j+1}) - G(t_{i,j})| = f(\epsilon_j)(t_{i,j+1} - t_{i,j})$, with ϵ_j in between $t_{i,j}$ and $t_{i,j+1}$. This is equivalent to $|t_{i,j+1} - t_{i,j}| = \frac{1}{f(\epsilon_j)(T_i - 1)} \leq \frac{c}{T_i - 1}$. For each $t \in \mathcal{T}^N$, there is precisely one interval $[t_{i,j}, t_{i,j+1})$ that

contains t , and since the interpolation process agrees with the observed curve on the time points $t_{i,1}, \dots, t_{i,T_i}$, it follows that for each curve $i = 1, \dots, N$, $0 \leq \rho(\tilde{\mathcal{Y}}_i^*, \hat{\mathcal{Y}}_i^*) \leq 2 \sup_{|s-t| \leq c/(T_i-1)} \|\hat{\mathcal{Y}}_i^*(t) - \hat{\mathcal{Y}}_i^*(s)\| \leq 2\omega_{\hat{\mathcal{Y}}_n^*}(\frac{c}{T_i-1})$, with $\omega_{\hat{\mathcal{Y}}^*}$ the modulus of continuity of $\hat{\mathcal{Y}}^*$. Since \mathcal{T}^N is compact and each function $\hat{\mathcal{Y}}_i^*$ ($i = 1, \dots, N$) is continuous, the function is also uniformly continuous with $\omega_{\hat{\mathcal{Y}}_n^*}(\frac{c}{T_i-1}) \rightarrow 0$ when $T_i \rightarrow \infty$ and $N \rightarrow \infty$. Since the sample of curves is i.i.d. and from Theorems 3.2 and 7.5 in Billingsley (2013), the random process $\tilde{\mathcal{Y}}_N^* \xrightarrow{P} \hat{\mathcal{Y}}_N^*$ converges as $T_s \rightarrow \infty$ and $N \rightarrow \infty$. From Theorem 3.1 in Billingsley (2013), $\tilde{\mathcal{Y}}_N^* \xrightarrow{P} \mathcal{Y}^*$.

(iii). Under the stated assumptions, Theorem 4.1 of Zuo & Serfling (2000b) yields the a.s. convergence of the β -trimmed regions $D_\beta(t, F_{\tilde{\mathcal{Y}}(t),N})$ to $D_\beta(t, F_{\mathcal{Y}(t)})$, together with a nesting property such that for $0 < \epsilon < \beta$, $D_\beta(t, F_{\mathcal{Y}(t)}) \subset D_\beta(t, F_{\tilde{\mathcal{Y}}(t),N}) \subset D_{\beta-\epsilon}(t, F_{\tilde{\mathcal{Y}}(t),N}) \subset D_{\beta+\epsilon}(t, F_{\mathcal{Y}(t)})$ for all $t \in \mathcal{T}$. From the dominated convergence, $\int_{t \in \mathcal{T}} |w_\beta(t; F_{\tilde{\mathcal{Y}}^*(t),N}) - w_\beta(t; F_{\mathcal{Y}^*(t)})| dt$ converges to 0 as $T_s \rightarrow \infty$ and $N \rightarrow \infty$ when w is proportional to the volume range. When w is proportional to t , $\int_{t \in \mathcal{T}} |w_\beta(t; F_{\tilde{\mathcal{Y}}^*(t),N}) - w_\beta(t; F_{\mathcal{Y}^*(t)})| dt = \int_{t \in \mathcal{T}} |g_{N,k}(t) - g(t)| dt \leq \sup_{t \in \mathcal{T}} |g_{N,k}(t) - G(t)| \xrightarrow{a.s.} 0$ from the Glivenko–Cantelli theorem.

2) The consistency of GMFED can be proven by the proof of consistency of ED in Narisetty & Nair (2016) under Conditions (A)–(E).

References

- Abalo, K. & Kostreva, M. (2005). Berge equilibrium: some recent results from fixed-point theorems. *Applied Mathematics and Computation*, 169(1), 624–638.
- Billingsley, P. (2013). *Convergence of Probability Measures*. John Wiley & Sons.
- Claeskens, G., Hubert, M., Slaets, L., & Vakili, K. (2014). Multivariate functional halfspace depth. *Journal of the American Statistical Association*, 109(505), 411–423.
- Etemadi, N. (2006). Convergence of weighted averages of random variables revisited. *Proceedings of the American Mathematical Society*, 134(9), 2739–2744.

- Narisetty, N. N. & Nair, V. N. (2016). Extremal depth for functional data and applications. *Journal of the American Statistical Association*, 111(516), 1705–1714.
- Zuo, Y. & Serfling, R. (2000a). General notions of statistical depth function. *Annals of Statistics*, 28(2), 461–482.
- Zuo, Y. & Serfling, R. (2000b). Structural properties and convergence results for contours of sample statistical depth functions. *Annals of Statistics*, 28(2), 483–499.